MagnetoRheological Dampers for Mass and Energy Sensitive Applications

by

Mohammad Mehdi Naserimojarad

M.Sc., Simon Fraser University, 2015

B.Sc., Shiraz University, 2012

Thesis Submitted in Partial Fulfillment of the

Requirements for the Degree of

Doctor of Philosophy

SIMON FRASER UNIVERSITY

Fall 2018

Approval

Name:	**Mohammad Mehdi Naserimojarad**
Degree:	**Doctor of Philosophy**
Title:	**MagnetoRheological Dampers for Mass and Energy Sensitive Applications**
Examining Committee:	**Chair: Amr Marzouk** Lecturer

Mehrdad Moallem
Senior Supervisor
Professor

Siamak Arzanpour
Senior Supervisor
Associate Professor

Edward Jung Wook Park
Supervisor
Professor

Shahram Payandeh
Internal Examiner
Professor
School of Engineering Science

Ramin Sedaghati
External Examiner
Professor
Department of Mechanical and
Industrial Engineering
Concordia University

Date Defended/Approved: December 5, 2018

Abstract

MagnetoRheological (MR) dampers have been used as reliable electronically adjustable shock and motion control devices in the past few years. Although these dampers have proven their performance in practice and the cost has decreased, their usage has been limited to high-end applications. The main drawback of MR dampers is their relatively large weight and energy consumption when compared to their passive counterparts. In this thesis, we investigate factors affecting weight and energy consumption of MR dampers and devise solutions to achieve energy-efficient and light-weight dampers. To this end, an analytic approach is presented to design and build a low-energy consumption and lightweight MR damper. It is shown that the proposed configuration can decrease the mass of MR damper significantly and reduce the energy consumption when AlNiCo alloys are utilized in the magnetic core. A proof-of-concept MR damper for mountain bike applications is designed, fabricated, characterized, and tested in the field, which meets the requirements in mountain bike industry in terms of energy consumption, compression and rebound forces, mass, size, and on-the-fly adjustability of the damping forces, by the user.

Keywords: Magnetorheological Dampers, Vibration Control, Optimal Design, Smart Materials

*To my life, my family***.**

Acknowledgement

I would like to acknowledge my senior supervisors Prof. Mehrdad Moallem and Prof. Siamak Arzanpour for their support and being a role model for me in professional research and ethics over the course of my PhD studies at Simon Fraser University. Also I would like to thank my examining committee including Prof. Edward Park, Prof. Shahram Payandeh and Prof. Ramin Sedaghati for their dedication and all the constructive suggestions to improve this thesis. I am grateful to financial and strategic sponsors of this project including NSERC and Rocky Mountain Bikes to fund this research and provide technical and scientific support. Specifically I would like to acknowledge Lyle Vallie, Tom Ferenc and Jaonne Hastie for all the knowledge and support they provided to make this research possible. Last but not least, I am grateful to all my colleagues at Motion and Power Electronics Control Lab at Simon Fraser University for years of friendship and help through my career to become a research scientist and achieve my PhD.

Table of Contents

List of Tables

List of Figures

Chapter 1. Introduction

MagnetoRheological (MR) technology, since its discovery in 50's[1], has been the baseline for several innovations in the engineering sectors such as automotive suspension systems [2]–[4], prosthetics [5]–[7], structural engineering [8], [9], and aerospace [10], [11]. This technology has proven its effectiveness as a reliable solution for motion and vibration control in commercial applications by being employed in shock absorbers, rotary brakes, elastomers, and clutches.

MR technology is based on MR effect that can be seen in MR fluid and MR elastomer. In both of these cases, micron-sized ferromagnetic particles are dispersed in a carrier medium, which is liquid in MR fluids and a polymer in MR elastomer. The main effect observed in MR fluid is an increase in the viscosity by applying an external magnetic field. In micro scale, the magnetic field brings the ferromagnetic particles together to form chains in the direction of the magnetic flux lines. The chain formation results in a limitation in the fluid-flow or surface movement that is seen as an increase in the viscosity or shear rate [1].

Until early 90's the biggest barrier to MR technology commercialization was the lack of advancements in control systems, microelectronics and sufficient funding for research and development [12], [13]. Since the mid-90s, with improvements in electronics and digital control systems, MR technology started to become widely employed in industrial applications. Moreover, the investments from compines such as Lord and Delphi accelerated the adoption of MR technology, by automakers for consumers and military purposes.

Not until very recently, due to relatively high prices of MR fluid, luxury and high-performance applications were the main areas of its application, and it was not very well received for mainstream commercial products. In other sectors of industry, although MR technology could significantly improve the performance, it was not widely commercialized not only because of its cost but also due to its power inefficiency and weights matters.

MR technology cost has significantly decreased in recent years because of advancement in the chemistry side and expiry of major patents. Although the prices have depreciated over time, MR technology has not found its way into new industrial applications due to the power consumption and weight. To overcome these barriers the aim and scope of this dissertation is to investigate new methods, technologies, and algorithms to make MR devices more efficient in terms of the energy consumption and lightness and make it market ready for weight and energy sensitive applications. It is necessary to recognize the sources of weight and power consumption inefficiencies and investigate methods and resolutions to address the issues.

1.1. Motivation of Research

The main two drawbacks of MR technology devices is power consumption and weight. MR dampers have higher weight comparing to its counterparts which are hydraulic and friction dampers. The main reason is the high density of MR fluid that consists of 80-90 weight percent of iron particles. Moreover, achieving bigger force range in MR dampers requires a wider active area of magnetic poles that results to a larger size of the piston and bigger reservoir for the MR fluid. As a result, designing MR dampers for applications with constrained mass and dimensions is a lot more challenging. Other than the mass inefficiency another major drawback of MR dampers is their energy requirements. MR dampers will require continuous electric current whenever a stiffness other than off-state

stiffness is required. This makes utilizing MR dampers very costly in terms of energy consumption. The side-effect to high energy requirements is requiring a bigger energy storage device. Considering the available battery technologies and the energy per KG they can provide, higher energy consumption means higher weight due to the weight of the battery.

The weight issue is usually addressed by optimizing the dampers to remove the excess parts that do not play a role in the hydraulics and magnetics. Different topologies and configurations are also studied to address the size and weight issue. A novel perspective that can indirectly result in weight and size reduction of the MR dampers is to maximize the dynamic range while constraining the weight and size of the damper in the process of design. This can be done by optimizing the conventional configurations for MR dampers or deploying novel configurations that can improve the performance.

There are two major approaches to tackle the energy consumption of MR dampers. The common approach that has been used in the optimal design of MR dampers is to minimize the resistive dissipation of the coil by investigating the energy consumption for different wire gauges considering the number of turns that can potentially be wounded in the space available for the electromagnetic coil. Using this method the joules of energy dissipated per weber of magnetic flux generated is calculated and most efficient wire gauge will be picked. This method cannot significantly reduce the energy consumption and alternative solutions should be investigated. The other solution that has recently attracted more attention among researchers is employing AlNiCo as a magnetic latch. Using AlNiCo will eliminate the need for continuous electric current that can significantly decrease the energy requirements while switching the state of the damper is not required very often. These solutions will be investigated in more details in the following chapters with the objective to design an MR damper for energy and mass sensitive applications.

1.2. A Review on The Background and Current Status of MR Technology

MR fluids are a group of smart materials that respond to the external magnetic field by increasing their shear rate/viscosity. An MR fluid consists of micron-sized ferromagnetic spheres dispersed in a carrier fluid. The carrier fluid can be a polar fluid such as water and alcohol, or a non-polar liquid such as synthetic oil, or any other hydrocarbon. Based on the type of carrier fluid, additives, which are usually surface active agents (surfactant), are added to stabilize the fluid and prevent sedimentation of particles [1].

When MR fluid is subjected to a magnetic field, the particles are magnetized into magnetic bipolar and align to form a chain of particles in the direction of the magnetic field as shown in Fig 1.1.

Since the fluid and the particles are stuck together by the surfactants, the formed chains can restrict the flow of the fluid. The restriction in the fluid flow is seen as an increase in the fluid viscosity or shear rate in the macro scale.

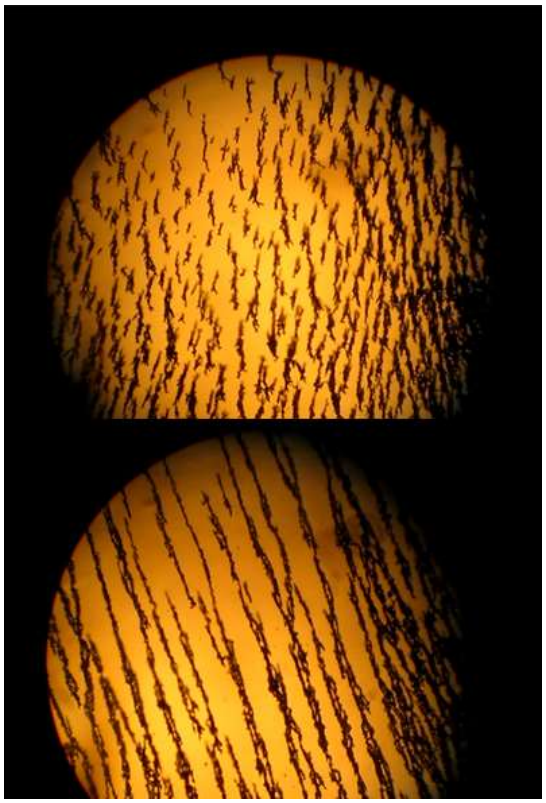

(a)

(b)

Figure 1.1 (a) MRF in the absence of a magnetic field, (b) MRF particle alignment under the influence of magnetic field.

1.2.1. MR Fluid Modes of Operation

As mentioned earlier the operation of MR fluid is all about chain formation and change in the viscosity of the fluid. An MR fluid can be used in three different modes including shear mode, squeeze mode, and valve mode. In this section, these three modes will be briefly explained.

Shear Mode

In the shear mode, two parallel plates are moving relative to each other, and the area between them is filled with MR fluid. Once the magnetic field is applied perpendicularly to the plates, the chain formation between the surface of the two plates causes a friction-like force that opposes the movement of the plates. This mode is

depicted in Figure 1.2. Shear mode is commonly applied in MR brakes and less regularly in MR dampers [14].

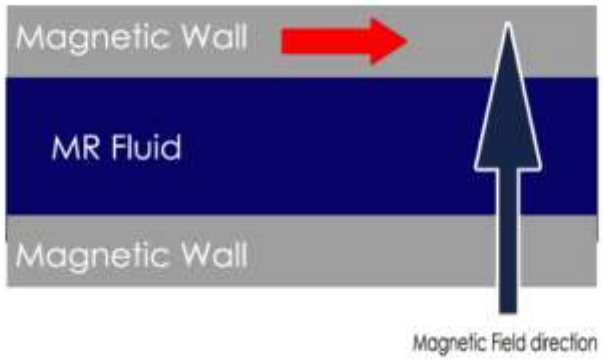

Figure 1.2 MR fluid operation in shear mode.

Squeeze Mode

Another mode of operation for MR fluids is the squeeze mode. In this mode, two plates are squeezed to each other, and the area between the plates is filled with MR fluid. By applying a perpendicular magnetic field, the chain formation opposes movement of the plates. This mode is mainly used in MR elastomers [12]. Figure 1.3 shows this mode of operation.

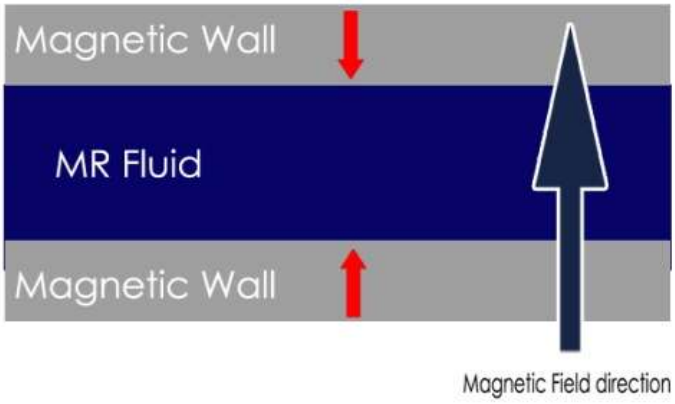

Figure 1.3 MR fluid operation in squeeze mode.

Valve Mode

In this mode, the MR fluid acts as a valve. The plates are fixed and the MR fluid is flowing in between. By applying the magnetic field in the vertical direction relative to the fluid flow direction,MR effect will excite the particles to form chains that constraints the fluid flow [12]. Figure 1.4 demonstrates how this mode of operation works.

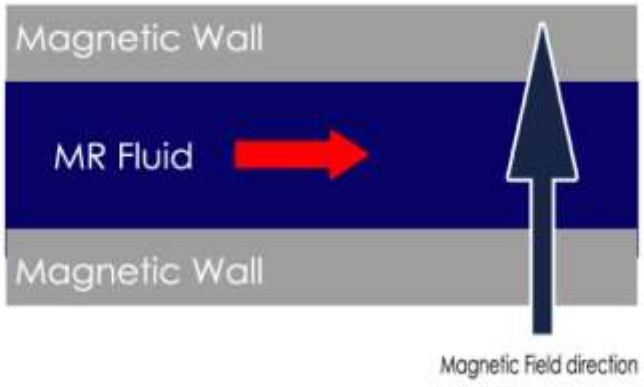

Figure 1.4 MR fluid operation in valve mode.

1.2.2. Types of Suspension Systems

Suspension systems are a necessary part of every vehicular system with the functionality to mitigate the shock and vibration and improve the handling of the vehicle. Suspension systems are divided into three groups including passive, semi-active and active suspension systems. Each of these systems has their own pro and cons. In this section, each of these technologies will be briefly explained.

Passive Suspension Systems

Passive systems are the most common type of suspension used for different types of vehicular systems such as automobiles, aircrafts, and bikes. In passive systems the

hydraulic force generated while the hydraulic fluid is pushed to pass through an orifice dissipates the kinetic energy. The biggest advantage of these systems is the simplicity, reliability, fail-safety and the fact they do not require batteries and electronics to function. The disadvantage though is that this type of suspension systems are not adjustable in real time thus the performance is not the best in every situation.

Active Suspension Systems

Active suspension systems are based on an actuator system that will adjust the stiffness and characteristics of the suspension to the system to fit the situation the vehicle is at. Active suspension systems while having a superior performance are known to have higher costs of maintenance and added complexity, which will increase the end-user price. The other drawback of active suspension systems is that these systems are prone to failure. With complex electrical and mechanical parts integrated together, active suspension systems have a higher probability of failure comparing to passive and semi-active suspension systems.

Semi-Active Suspension Systems

Semi-active suspension systems are a mixture of both worlds. These systems are highly similar to passive systems while having the ability to adjust their characteristics in real time. The most common type of semi-active dampers are MR dampers that more or less are similar to conventional passive dampers. This makes MR damper fail-safe as if there is a failure in the control systems the damper will function as a conventional hydraulic damper.

1.3. Summary of Contributions and Outline of This Dissertation

The aim in this research is to optimally design magnetorheological damper for applications where weight, space and energy consumption is a concern. In this regards it is necessary to investigate optimal design approaches, alternative configurations and redesign MR dampers in a way that they fit real world applications. To achieve the objectives the three major contributions have been made that are listed as follows.

1. A comprehensive approach for optimal design of MR dampers
2. A novel configuration for MR dampers that minimizes the weight and dimensions of the damper while utilizing solutions to optimize energy consumption.
3. A novel configuration for MR dampers with asymmetric damping characteristics that addresses the damping requirements for industrial applications such as automotive and mountain bike industry.

The summary of each chapter in addition to highlight of contributions is discussed in the following sections.

1.3.1. Chapter 2: Modeling and Optimal Design of MR Dampers

The modeling of MR dampers is explained in chapter 2. Different modeling methods are discussed in this chapter and quasi-static as a reliable and trusted method of modeling for design purposes is introduced. The suggested modeling scheme is employed in this chapter to develop a design approach based on genetic algorithm. The cost function of the optimal design problem is set in a way to minimize the overall mass

while maximizing the dynamic range of the damper subject to various constraints such as avoiding magnetic losses and keeping the off-state force in a certain range.

1.3.2. Chapter 3: A Comprehensive Approach for Optimal Design of MR Dampers

Employing the lessons learned from chapter 2, a novel comprehensive approach for optimal design of MR dampers is developed in this chapter. The proposed optimal design approach utilizes analytic methods along with Finite Element Analysis (FEA) to obtain the best global optimum solution for MR dampers with multi-material structures with given specifications such as length of piston, off-state force and cylinder radius. The proposed design approach is employed to optimally design and fabricate an MR damper with AlNiCo core. The experimental results of the fabricated damper characterization are compared with the ones obtained from simulation and it is shown that the results match with an slight error.

1.3.3. Chapter 4: Alternative Configurations for Low-Energy, Low-Mass MR Dampers

Conventional MR damper configurations have not been able to fulfill the requirements for applications with mass, size and energy limitations. This has led to less adoption of the MR technology ion those applications. In this chapter, alternative topologies for MR dampers are studied and a novel configuration for MR dampers is proposed. The proposed configuration utilizes the entire length and surface of the MR damper pistons active magnetic area of contact that minimizes the mass and space loss. The proposed configuration is compatible with AlNiCo core that helps to minimize the energy consumption and excess heat generation. To verify the superiority of the proposed design it was optimally designed along with a conventional MR damper with similar weight,

size and characteristics utilizing the design approach explained in chapter 3. It was shown using experimental results that the proposed design, called Zebra, is able to beat the dynamic range of MR dampers by 100%.

1.3.4. Chapter 5: MR Dampers with Asymmetric Damping Behavior

In real world applications it is required that the dampers provide three to five times more force on the rebound side comparing to compression side. However in the academic researchers done on MR dampers this necessity have been ignored. In this chapter and novel configuration for MR dampers with asymmetric damping behaviors will be proposed. An MR damper is designed and fabricated using the proposed configuration for downhill mountain bike application. The MR damper is characterized on an experimental setup along with a commercial damper of the same size and dimensions. The results will be compared and the behavior of the two dampers will be analyzed. It is shown that the proposed configuration is able to match and beat the characteristics of the commercial damper while bringing the controllability and features of MR dampers into effect.

1.3.5. Chapter 6: Summary, Conclusion and Suggestions for Future Works

The research work in this thesis is summarized in this chapter. Based on the theoretical, simulation and experimental studies done in this research a conclusion is made and further suggestion to enhance the outcome are proposed to be done as future works.

Chapter 2. Modeling and Optimal Design of MR Dampers

2.1. Introduction

Several authors using recursive search and analytical approaches have studied performance optimization of MR devices. In [9-11], the authors used the ANSYS optimization toolbox to optimally design the magnetic structure of their damper. This method has been utilized in the design of several different MR devices such as brakes, dampers, and valves. In [12], the authors used the simulated annealing method to optimally design an MR brake. The simulated annealing algorithm is inspired by an industrial process of heating a metal and cooling it down slowly to decrease deficiencies in the metal part. Although simulated annealing is a useful method, it does not guarantee convergence to the optimum point. A multi-objective genetic algorithm was used in [13] to optimally design an MR damper. The multi-objective genetic algorithm is a powerful method to optimize complex systems; however, it is computationally complex and can take several iterations to reach the solution. Moreover, this method does not guarantee whether the solution is a local or a global optimum. All of the aforementioned methods are based on numerical or recursive search methods for obtaining the global optimum solution. There have also been several analytic studies on the optimal design of MR dampers. Analytical design of MR devices is a challenging problem due to their multiphysics nature and non-linearities (e.g., see [14],[15]). A shortcoming of these methods is that they can become quite complex, especially for more advanced configurations and multi-material structures such as MR dampers with built-in controllable permanent magnets, known as AlNiCo [16].

In this chapter MR damper modeling methodologies for will be studied for optimal design purposes.

2.2. MR Damper Operation and Mechanism

Any hydraulic damper consists of a piston that moves in a cylinder. Figure 2.1 shows the diagram of a commercial MR damper. The kinetic energy of the system is dissipated in the fluid that passes through the orifices in the piston. The amount of dissipated energy is dependent on the viscosity of the fluid that passes by the piston's annular duct and the speed of movement. In MR dampers, the piston is equipped with a magnetic circuit that can change the viscosity of the fluid that is passing by the piston's annular duct by adjusting the electric current. Considering the magnetic valve in the micro-scale and applying current to the coil results in the magnetic field to form chains of bipolar magnetic particles. The change in the fluid viscosity will then result in a change of the damping characteristics of the damper.

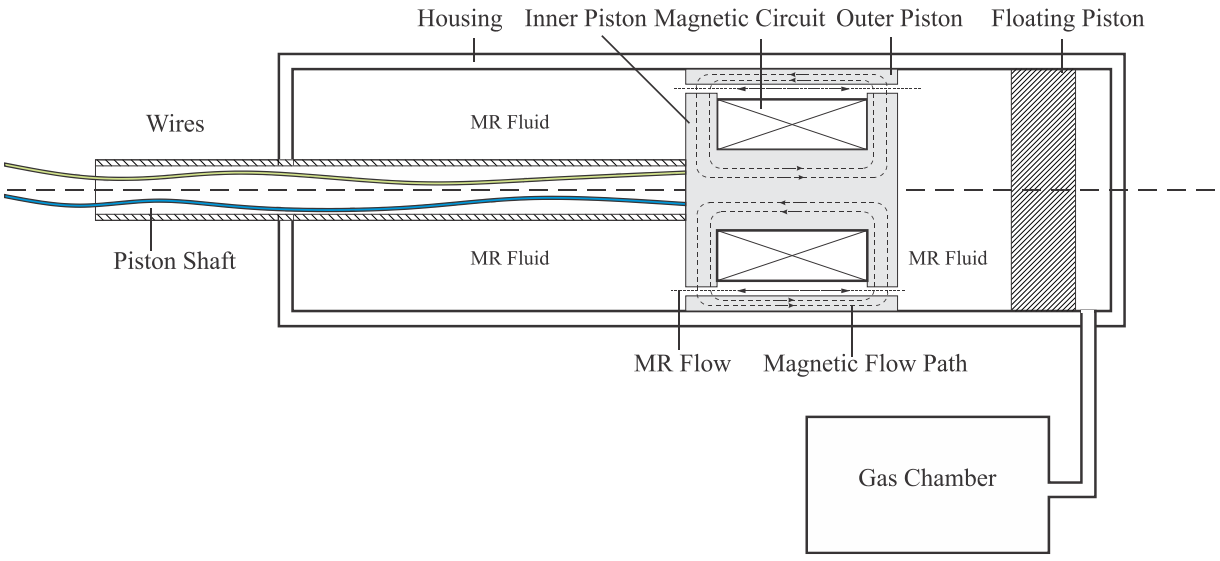

Figure 2.1 Schematic of an MR damper.

As it can be seen in Fig 2.1, the cylinder is divided into two chambers with a floating piston in between. The fluid chamber is filled with MR fluid and the piston moves in this chamber. The gas chamber is filled with air or pure nitrogen and its functionality is to compensate for the increase in the volume of the fluid chamber when the shaft enters the fluid chamber.

2.3. Modeling of MR Dampers

Several methods have been proposed for modeling MR dampers [15]–[18] that can be used to simulate, design, and control MR dampers. However, in addition to high accuracy, a suitable model for design should be able to relate damper performance to physical dimensions and fluid characteristics. In this work, we utilize the modeling technique presented in [13],[14], in which the total force of MR damper is separated into three parts: Gas chamber force, hydraulic force, and MR effect force. This method of modeling is very well accepted in the research community for being accurate and justifying the experimental behaviour with physics and dimensions. This model is called quasi-static modeling.

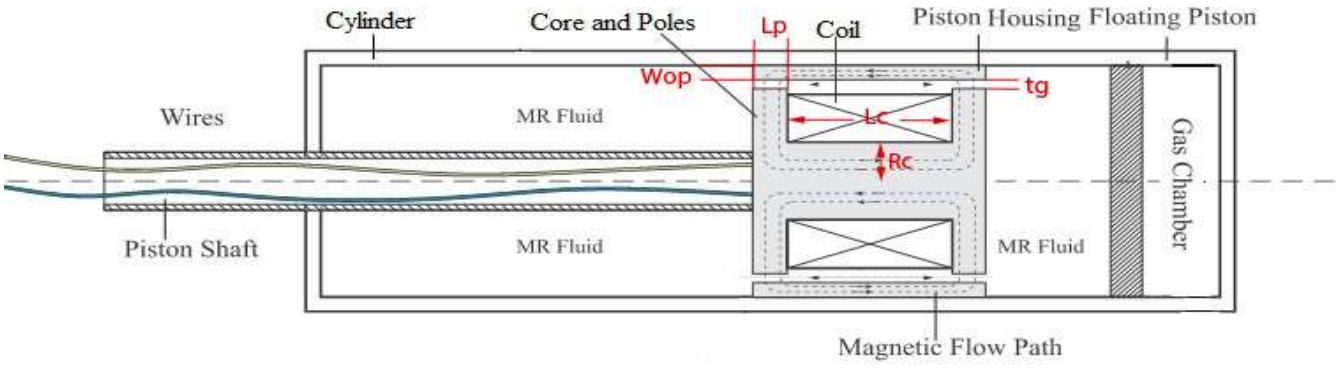

Figure 2.2 MR damper schematic.

Referring to Fig. 2.1, the following relationships can be obtained

$$F_g = A_s P_a = A_s P_0 \left(\frac{V_0}{V_0 + A_s x_p}\right)^{\gamma} \quad (2.1)$$

$$F_{vis} = \frac{12\,\eta L}{\pi {t_g}^3 R_d}\left(A_p - A_s\right)^2\left(\dot{X}_p\right) \quad (2.2)$$

$$F_{MR} = 2c\frac{L_p}{t_g}\,\tau_y\left(A_p - A_s\right)sgn\left(\dot{X}_p\right) \quad (2.3)$$

The various parameters in formulas (2.1) – (2.3) are defined in Table.2.1.

Table 2.1 Parameters definition for formulas (2.1) – (2.3).

Parameter	Statement	Parameter	Statement
F_g	Hydraulic force	F_{vis}	Viscous Force
A_s	Cross section area of the shaft	F_{MR}	MR effect force
P_a	Pressure of gas	C	Fluid flow velocity dependent variable
P_0	Initial pressure	L_p	Length of magnetic pole
V_0	Initial volume of the gas chamber	τ_y	Yield stress
X_p	Position of the piston	A_p	Area of the piston
γ	Coefficient of thermal expansion	R_d	Average radius of the fluid flow gap
η	Viscosity of the fluid	t_g	Thickness of fluid flow gap
L	Length of the piston		

2.4. Model Verification and Validation

The model discussed in section 2.2 has been used widely for design purposes [15], [16] and [19]. However, there is no information available about how accurate this model is. In this section, we will investigate the accuracy of this model by simulating a

commercial damper and comparing the results with experimental data of the same damper. The LORD 8040 damper was selected for this purpose. The parameters of this damper are shown in Table 2.3. A picture of this damper is shown in Fig 2.3.

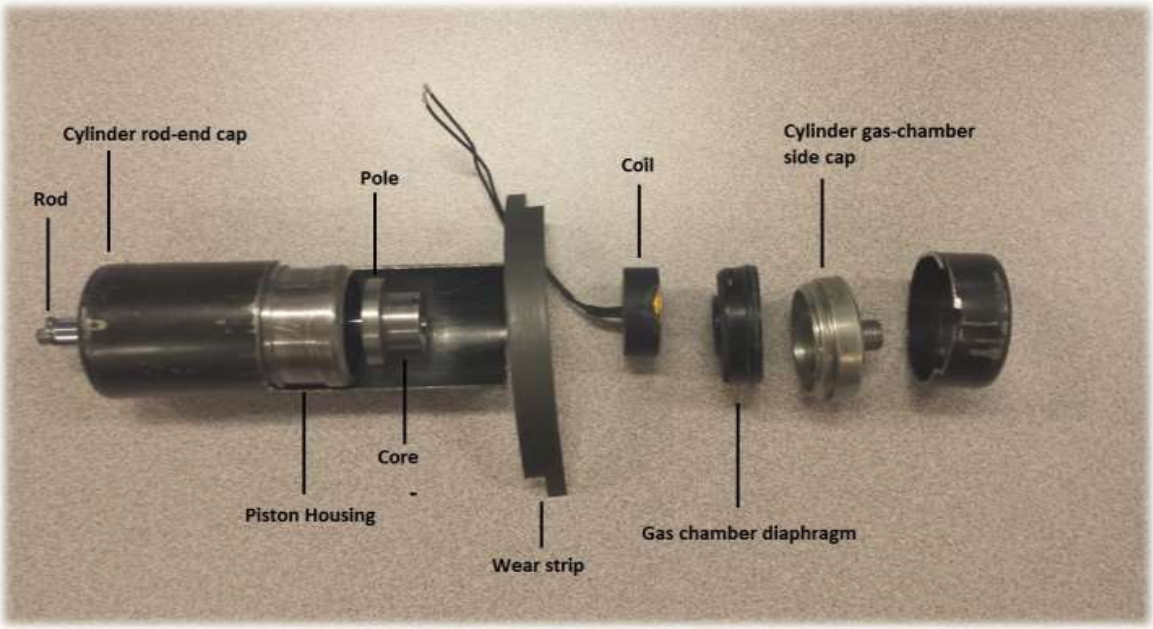

Figure 2.3 Exploded view of LORD8040 MR damper.

The magnetic structure of the MR damper was modeled in the COMSOL-Multiphysics with the physical properties mentioned in Table 2.2. COMSOL is a Finite Element Analysis (FEA) software that is capable of calculating different physical parameters. At this stage, we took advantage of this software to calculate the magnetic field intensity in the MR fluid in order to calculate the yield stress which is a function of magnetic field. Figure 2.4 Shows the FEA result of Lord MR Damper in electric current equal to 0.8 A.

Table 2.2 Specififcations of the Lord 8040 commercial damper.

Value	Parameter
MRD-8040	Commercial Name
MRF 122EG	MR Fluid Name
0.042 P.S	Fluid Viscosity
20.8 mm	The outer diameter of the cylinder
19.4 mm	Inner Diameter of Cylinder
0.65 mm	The thickness of gap (tg)
14.575 mm	The median radius of the gap (distance of center and middle of the gap)
5.1 mm	Pole length (Lp)
5 mm	Shaft Diameter
11 mm	Core Length (Lc)
10 mm	Core Radius(Rc)
3 mm	Thickness of outer piston

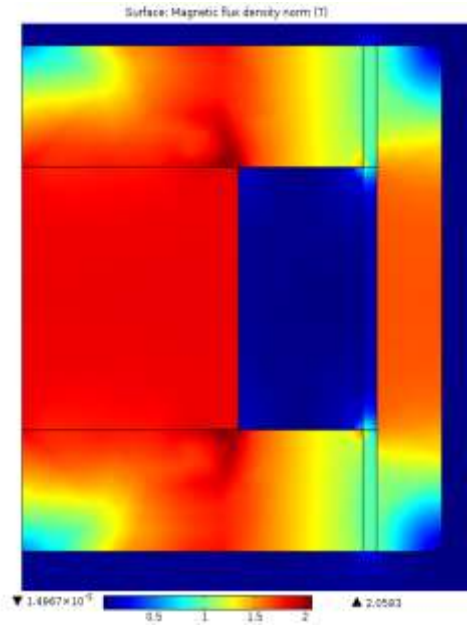

Figure 2.4 FEA analysis for LORD 8040 damper.

Using the information obtained from FEA and the model given by (2.3), (2.4) and (2.5), the damper force at 3 different speeds (0.11, 0.30,0.48 m/s) and two different electric currents (0,0.8A) were calculated. The results can be seen in the third column of Table 2.3. The force varies between 158.6N in low speed and no current to 1489.6 N at the highest speed and 0.8A .

In order to compare the calculated forces with experimental results, the damper was tested in the mentioned speeds and currents using a hydraulic shaker by MTS. The picture of the experimental setup can be seen in Fig 2.5. The results obtained from testing the damper are shown in Figure 2.6.

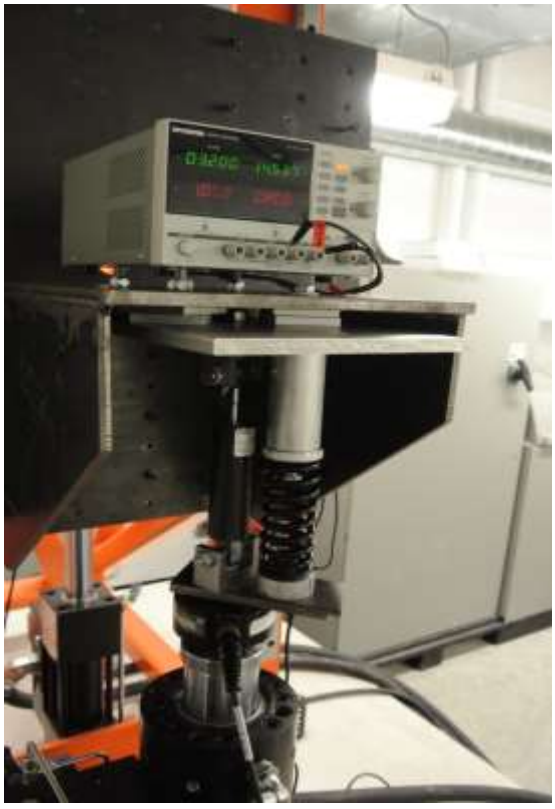

Figure 2.5 LORD 8040 damper test setup.

The modeling error in lower speed is 1% when the current is zero and it is about 2% when current is applied to the coil. By increasing the speed from 0.11 m/s to 0.48 m/s the error is increased from 1% to 3% for no current, and from 2% to 4.5% for 0.8 A current.

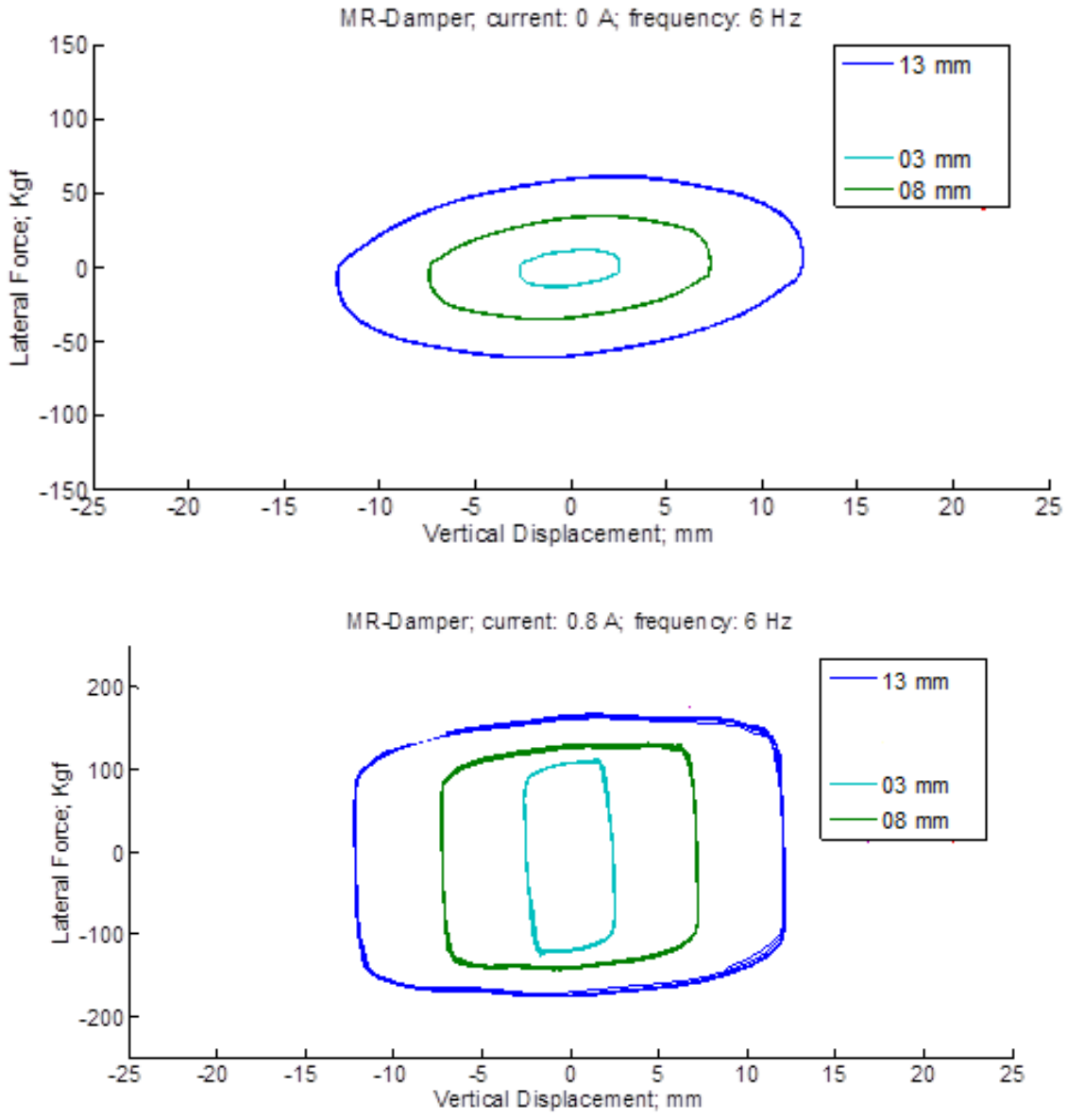

Figure 2.6 Force-velocity and force-displacement graphs for LORD 8040 damper.

As expected, at lower speeds this model is more accurate. As the speed increases, the fluid flow gets closer to turbulent regime and doesn't follow the laminar fluid flow and ideal gas model assumptions considered in formulas (2.3)-(2.5). However, we will consider the 4% error reasonable in this study and will rely on this model for representing the physical properties effects on the behavior of the damper.

2.5. Optimal Design of MR Dampers Using Genetic Algorithm (GA)

Optimal design is a critical stage in any design problem. In general, the goal of any design optimization problem is minimizing undesired situations while maximizing the desired ones. For example, in a mechatronic control system, the design goal might be to minimize the power consumption and control effort and maximize the error performance of the system. In this research, our goal is to minimize the total weight and power consumption of a MR damper while maintaining the performance (damping force) within a specified range.

There are many different methods for optimal design and optimization of a system. These methods can be generally categorized into two groups, i.e. analytic and random optimization methods. Analytic methods are based on solving the mathematical model of the system to maximize a special feature. These methods are sometimes done graphically to implement the constraints on the calculations. Although these methods are highly efficient, it is not always easy to use them in a multi-variable optimization problem with nonlinear elements and constraints.

Random optimization methods are inspired from a natural effect or system such as ants' colony algorithm which is inspired from ants' endeavor in looking for food, or Genetic Algorithm (GA), which has been inspired by the evolution theory in genes. GA is considered as a powerful method for optimal design of complex systems in the past decade [20]–[23] specially for MR devices [24]. Because of its abilities and unique features for complex systems, we have chosen this algorithm to be used for optimal design in this study.

Many works have already been done on optimizing MR devices and structures. For example, in [24] a GA was used for optimizing a MR brake. In [15], [25], [26] the ANSYS optimization toolbox was used for optimal design. In the aforementioned works, the optimization goal was to increase the dynamic range and decrease the time constant. However, in this research our goal is to minimize the weight in order to design a MR damper for application that weight is an issue such as biomedical systems and mountain bikes.

In this chapter, the optimal design and simulation of MR dampers will be presented.

2.5.1. Genetic Algorithm

As it was mentioned earlier, GA is inspired by natural evolution theories. This algorithm was first introduced by John Henry Holland in 1975 in a book named "Adaptation in Natural and Artificial Systems" and since then it was used in different industrial and scientific applications [36].

The goal in GA is to maximize (or minimize) a function, called fitness function or cost function. Fitness function is usually a dimensionless function, comprising one or more

parameters, that are normalized to be comparable. For instance, a fitness function can take the following form

$$\text{Objective Function} = \frac{P_1}{a} + \frac{b}{P_2} \tag{2.4}$$

If our intention is to maximize this function, then P_1 is a parameter that we want to maximize, that is normalized with constant "a", and P_2 is a parameter that we want to minimize, which has been normalized with constant "b" [27].

GA requires an initial population that can be chosen randomly (or with a special strategy) based on the constraints of the optimization problem. Some members of this population will be chosen based on the fitness value to do the reproduction. There are some methods for choosing the members for reproduction. One of the most common methods for selection is the roulette wheel method, in which a roulette wheel will be divided into some sectors and the area of each sector represents the fitness function of each member. The roulette wheel starts to rotate (virtually) and members will be chosen randomly using the wheel. In this method, a fit member is more likely to be chosen such that the chosen members can produce better children for the next generation. The chosen members will get married by some methods such as cross-over and procedures such as mutation. This procedure continues until a stopping criterion is achieved. The stop criteria can be one of the following:

- The fitness criterion is achieved
- Number of generation achieves the limit
- Time limit

- Fitness difference between members diminishes so that no better generation is produced

In this research we will use MATLAB optimization toolbox to solve the optimal design problem.

2.5.2. Simulating MR Damper in COMSOL

COMSOL-Multiphysics is a Finite Element Analysis (FEA) software that is able to solve multiple physical problems at once. In this research we take advantage of its DC/AC magnetics module to simulate magnetic structure of MR dampers.

In FEA we can simulate and solve a structure in three different ways based on its shape: a) 3D b) 2D c) 2D Axisymmetric.

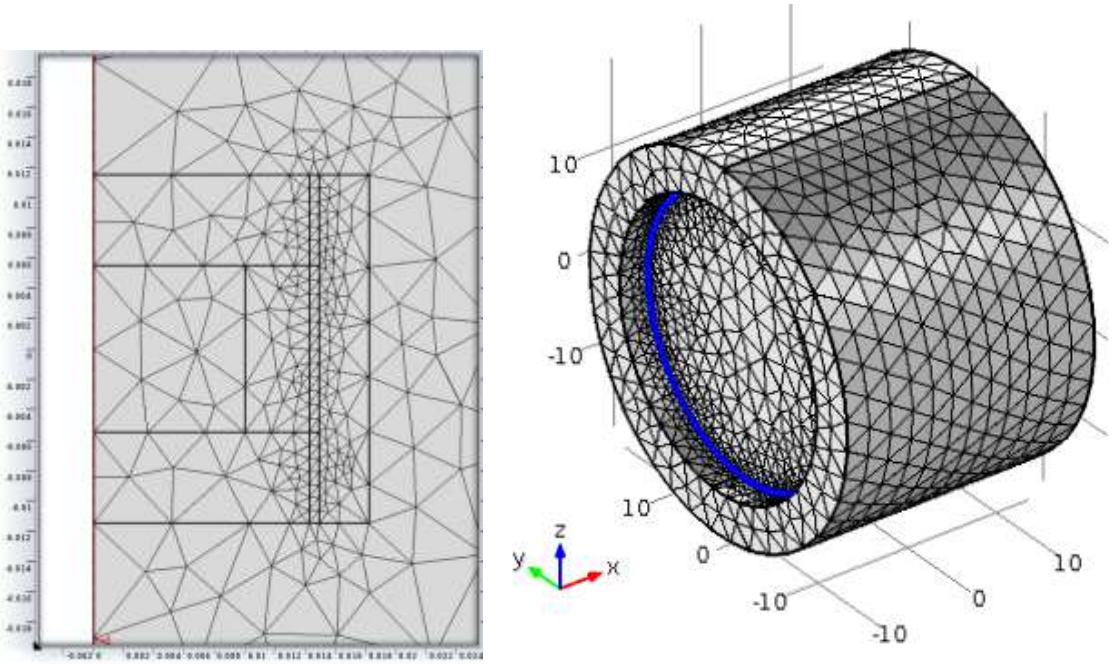

Figure 2.7 Meshed 2D axisymmetric model(left) and 3D model (right) of MR damper piston in COMSOL.

It is obvious that 3D analysis is the most accurate and most time consuming method. In this research, after doing the simulation with all of these methods we finally decided to use 2D axisymmetric method. The meshed 2D axisymmetric and 3D model of an MR damper can be seen in Fig 2.7.

In order to model the MR damper, the magnetic characteristics of materials should be modeled and imported into COMSOL. In our design, the MR fluid and Iron are the only magnetic materials and other materials are considered to have no magnetic properties. The B-H curve of MR fluid and Steel are shown in Figure 2.8.

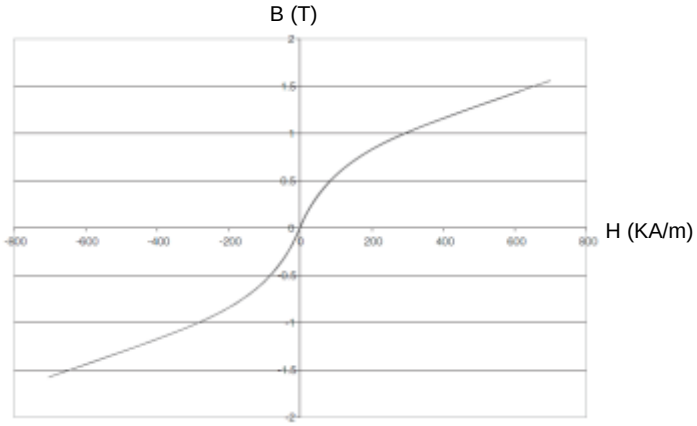

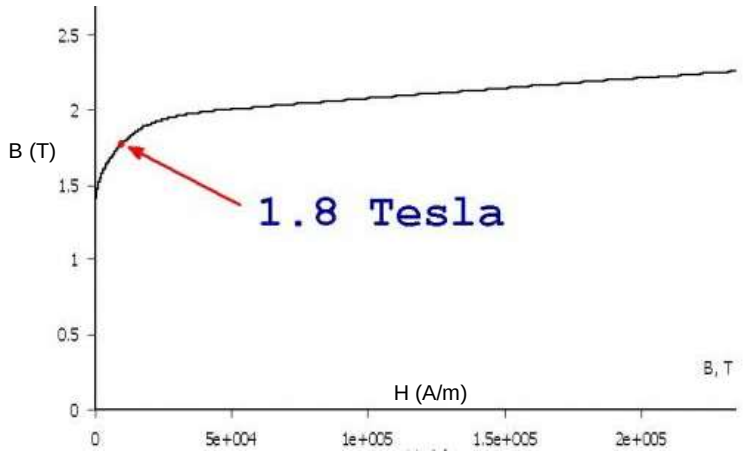

Figure 2.8 Magnetic characteristic curve for MR fluid(top) [28] and steel (down) [29].

An effect that is usually seen in magnetic materials is saturation, which means that after a certain value of magnetic field intensity, the rate of change in magnetic field density will decrease. The saturation point in steel is shown in Figure 2.8 that happens at magnetic flux density of about 1.8T. Magnetic saturation is a limitation that should be considered in designing a magnetic structure in order to avoid unnecessary power consumption.

After a sketch of the damper in COMSOL was drawn and the materials were defined, the model is ready to be solved. In order to do so, we defined some variable parameters in COMSOL, that could be used by MATLAB optimization toolbox for optimization.

The quasi static model presented earlier in this chapter was used in the COMSOL model to calculate the forces of the damper.

The relationship between τ_y and magnetic field intensity was extracted form the curve provided by Lord as shown in Figure 2.9 for commercial MR fluid 132DG.

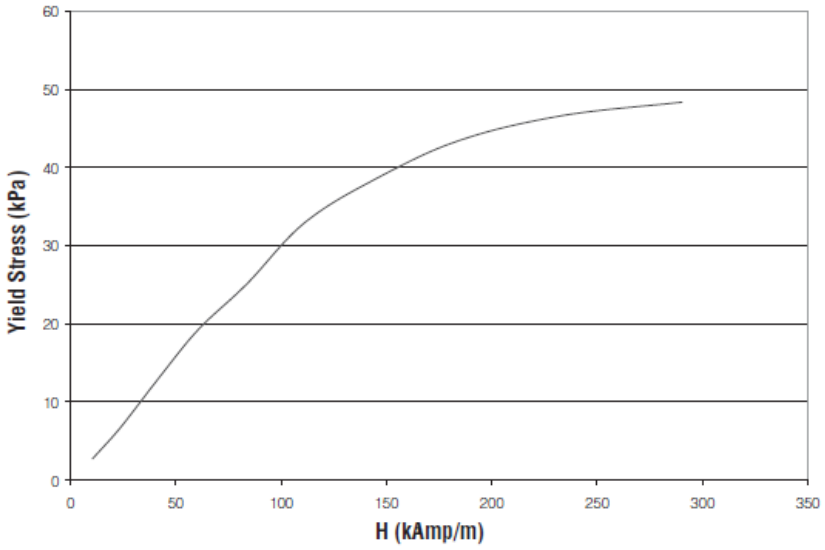

Figure 2.9 Yield stress versus magnetic field intensity curve [28].

To import the information of the curve in Figure 2.9 into MATLAB, a curve fitting was done with the following third order polynomial

$$\tau_y = p(H_{mr}) = C_0 + C_1 H_{mr} + C_2 {H_{mr}}^2 + C_3 {H_{mr}}^3 \quad (2.5)$$

after the completion of the fitting procedure $C_0, C_1, C_2 \ and \ C_3$ were found as 0.3, 0.42, -0.0012 and 1.05e-6 [15].

2.5.3. Optimal Design of MR Damper

So far, the optimization algorithm and the modeling procedure are explained. The next stage will be connecting these two tools and run the optimization algorithm with the model. to do so, the COMSOL-Livelink package for MATLAB was used to generate an m-file that works like a COMSOL simulation in MATLAB workspace. The variable parameters in the design are shown in Figure 2.10.

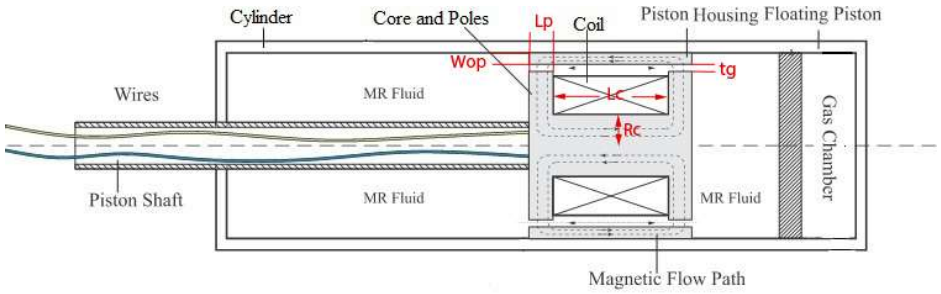

Figure 2.10 Optimization parameters definition.

As mentioned at the beginning of this chapter, in this study we are looking into minimizing the weight and maximize the dynamic range. To this end, let us define the dynamic range as,

$$\lambda_d = \frac{F_\eta + F_{mr}}{F_\eta} \tag{2.6}$$

To calculate the weight, the volume of each part can be multiplied to its corresponding density. The following formula is used to obtain the mass,

$$M = \pi\rho_{iron}\left(\left(R_{ic}^2 - R_{inp}^2\right)L_{piston}\right) + \left(2R_p^2\, L_p\right) + \left(R_c^2\, L_c\right)) + \pi\,\rho_{cooper}(\left(R_p^2 - R_c^2\right)L_c)) \tag{2.7}$$

In (2.7), ρ_{iron} and ρ_{cooper} are representing the density of Iron and Copper respectively. Here the mass of the piston is calculated since it is the only part we are optimizing. Eventually the fitness function to be minimized is given by,

$$Objective\ Function = w_m\left(\frac{M}{M_{desired}}\right) + w_\lambda\left(\frac{\lambda_{desired}}{\lambda}\right) \tag{2.8}$$

In (2.8), the parameters w_λ and w_m are used to adjust the importance of each parameter in the fitness function. The objective function used for optimization is as follows:

$$Objective\ Function = \ 0.7\left(\frac{M}{0.8}\right) + 0.3\ (\frac{4}{\lambda}) \tag{2.9}$$

As it can be seen in (2.9), weight minimization is more important for us in comparison to dynamic range maximization.

To prevent magnetic saturation and avoid unfeasible solutions, some constraints were added to the optimization problem as shown in Table 2.3.

Table 2.3 Optimization problem constraints.

Parameter	Constraint	explanation
Rc	$0.004m \leq R_c \leq \ 0.008m$	**Radius of core**
Lc	$0.006m \leq L_c \leq \ 0.02m$	**Length of core**
Lp	$0.002m \leq L_p \leq \ 0.015m$	**Length of pole**
Tg	$0.0004\mathrm{m} \leq \mathrm{t_g} \leq \ 0.0015\mathrm{m}$	**Thickness of gap**
Wop	$0.002\mathrm{m} \leq \mathrm{W_{op}} \leq \ 0.0045\mathrm{m}$	**Outer piston Wall thickness**
Acoil	$25\mathrm{m}m^2 \leq A_{coil}$	**Coil cross section area**
Lpiston	$0.05\mathrm{m} \leq L_{piston}$	**Length of piston**
Bmax	$B_{max} \leq \ 1.8\ \mathrm{T}$	**Max Magnetic field density**
Dynamic Range	$3 \leq Dynamic\ range$	**-**
Fpassive	$0.9\ F_{desired} \leq F_{passive} \leq \ 1.1\ \mathrm{F_{desired}}$	**Off-State force**
R_{ic}	15.875 mm	**Inner radius of the cylinder**

For the optimization algorithm some stop criteria were set that are shown in Table 2.4.

Table 2.4 Optimization stop criteria.

Criterion	Value
Number of Generations	**Inf**
Time limit	**Inf**
Fitness function limit	**Inf**
Stall generations limit	**50**
Stall time	**Inf**
Fitness function variations	**1e-3**

2.5.4. Results and Discussion

The optimization was run and the results in Table 2.5 were obtained. As it can be seen in Table 2.5, the magnetic field density does not go above the constraints and the dynamic range is in a reasonable range.

Table 2.5 Optimization results.

Design Variables			Characteristics	
Parameter	Initial Value	Optimal Value	Parameter	Optimal Value
Rc	$0.008\ m$	0.0089 m	$Max\ damping\ force\ F_{total}$ @ 0.5m/s	$1750\ N$
L_c	$0.012\ m$	$0.0145m$	$AverageB_{mr}$	$0.849\ T$
L_p	$0.008\ m$	$0.0051m$	Max B	$1.871T$
t_g	$0.001\ m$	0.0008 m	$Dynamic\ range\ \lambda$	4.6
W_{op}	$0.004\ m$	0.0042m	$Weight\ M$	$785\ g$

Based on the fitness function that was chosen for this study, the results do not represent the lightest design or the design with the highest dynamic range.

In Figure 2.10, the FEA result is shown for the optimized damper. In this figure, the red areas represent the parts with higher magnetic field density.

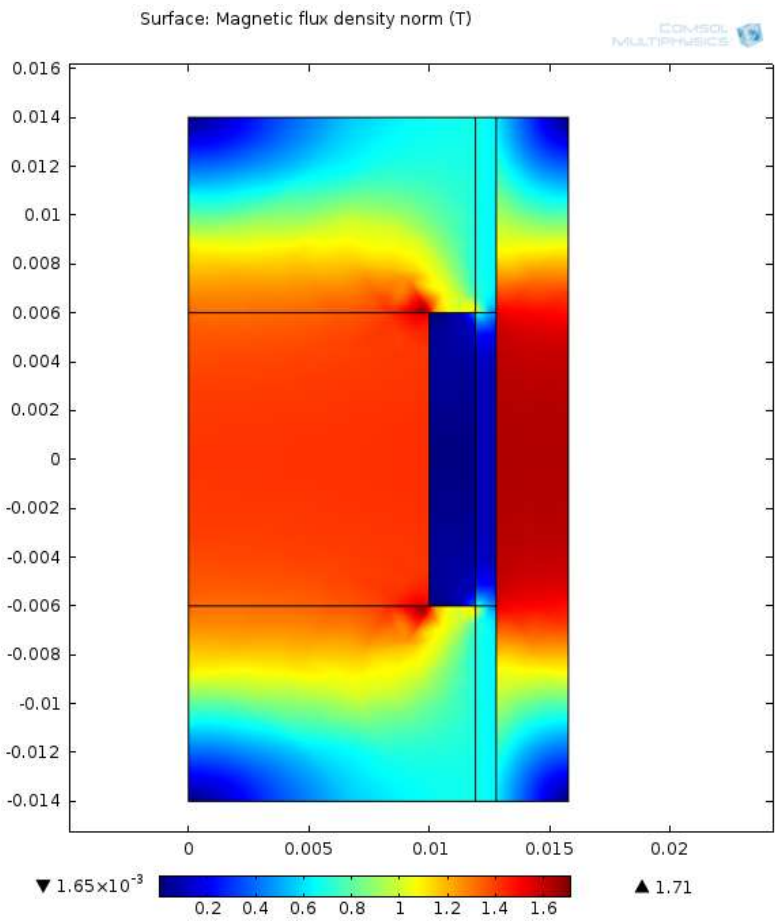

Figure 2.11 Designed MR damper finite element analysis.

After performing the optimization, the coil parameters should be calculated. At this stage, there is a groove that the coil can be wounded on. The cross section of the coil was calculated to be a 1.9 mm to 14.5mm rectangle. Different sizes of wire can affect the performance of the whole system. In Table 2.6, different parameters for different sizes of wire have been compared. The number of wire layers should be an even number so that the wire enters and exits the coil from the same side.

Table 2.6 Coil optimization results.

	AWG 24	AWG 25	AWG 26	AWG 28	AWG 30
Resistance of wire (Ω/m)	.084	.106	.1338	.2128	.3384
Max current (A)	3.5	2.7	2.2	1.4	.86
Layers of wire	4	4	4	6	8
Maximum wire turns	146	204	223	342	571
Length of wire (m)	5.36	5.88	6.47	12.44	21.03
Resistance of coil (Ω)	.449	.622	.869	2.64	7.09
Power consumption (W)	5.50	4.53	4.2	5.18	5.24
Inductance (H)	.004	.0075	.0096	.023	.0631
Time constant (Sec)	.009	.0121	.0111	.0087	.0089
NI	511	550.8	490.6	478.8	491

In Table 2.6, the length of wire in each layer was calculated and added together to find the whole length. By finding the wire length and using the wire datasheet, the resistance of the coil was found and the power consumption was calculated.

The Calculation of inductance is more involved since it depends on the structure of magnetic circuit and materials. To find an accurate value for inductor, the FEA software was used. In FEA, the total magnetic flux passing a section of the circuit was calculated and by using the formula below the inductance was calculated:

$$N\varphi = LI \qquad (2.10)$$

In (2.10), N is the number of turns, φ is the magnetic flux obtained from FEA, L is the inductance and I is the current passing through the coil.

After finding the inductance and resistance of the coil, the time constant of the coil can be calculated. In practice, the system response time is about four to five times of the time constant [30]. For a resistive-inductive load, the time constant is defined as follows

$$\tau = \frac{L}{R} \tag{2.16}$$

Finally, the parameter NI was calculated to have a reference to compare magnetic field strength produced by each of the coils.

2.6. Conclusion

The focus of this chapter was on different features of optimal design for MR dampers. First of all, the genetic algorithm was utilized as a powerful optimization tool in order to optimize the magnetic structure of a MR damper. In this stage, the piston was modeled in COMSOL. Afterwards, using Matlab-COMSOL LiveLink, Matlab Optimtool was used to apply genetic algorithm on the COMSOL model. finally, based on the results obtained from the optimization stage, an optimal design strategy for coil was proposed that takes different features of coil such as power consumption, time constant, and magnetic field strength into account.

Chapter 3. A Comprehensive Approach for Optimal Design of MR Dampers

3.1. Introduction

MagnetoRheological (MR) fluid is a ferro-fluid made up of ferromagnetic particles dispersed and stabilized in a carrier fluid. The dispersed particles, when subjected to a magnetic field, form chains in the direction of the magnetic flux lines and increase its viscosity by resisting the flow of the fluid. This unique property is utilized to make adjustable hydraulic devices called MR devices. These devices have been utilized in industrial applications including automotive suspension systems [3], [31], [32], civil structures [20], [33], [34], and biomedical systems [35], [36].

Performance optimization of MR devices has been studied by several authors using recursive search and analytical approaches. ANSYS was used in several works as the optimization toolbox for designing the magnetic structure of dampers[25], [26], [37].This method has been applied to design a variety of MR devices such as brakes, dampers, and valves. In [38] simulated annealing method was used to design an optimal MR brake. The simulated annealing algorithm is inspired by an industrial process of heating a metal and cooling it down slowly to decrease deficiencies in the metal part. Although stimulated annealing is a useful method, it does not guarantee convergence to the optimum point. Response surface method was proposed in [39] for optimal design of MR dampers. This method suggests a solution to find the global optimal parameters in a

computationally efficient way. A multi-objective genetic algorithm was used in [40] to optimally design an MR damper which is a powerful method to optimize complex systems. However, the method is computationally complex and does not guarantee reaching a local or global optimum. All of the aforementioned methods are based on numerical or recursive search methods for obtaining the global optimum solution. There have been several analytic studies on optimal design of MR dampers. Optimization based on analytical approaches is challenging due to the multi-physics nature and non-linearities involved in MR dampers (e.g., see [41], [42]). Another shortcoming of those methods is that they can become quite complex, especially for more advanced configurations and multi-material structures such as MR dampers with built-in controllable permanent magnets known as AlNiCo [43]. Thus a comprehensive design approach for optimal design of MR dampers that can be utilized in practical applications is highly required.

In this chapter, we present an analytic MR damper optimal design approach for complex and multi-material structures. Considering the manufacturing limitations and practical specifications, the proposed method guarantees feasibility of the final solution and can significantly simplify the optimization process and reduce the computational complexity.

3.2. Modeling of MR Dampers

Several methods have been proposed for modeling MR dampers hat can be used for simulation, design and control purposes [15]–[17] . However, a suitable model for the design purposes should be able to relate damper performance to its physical dimensions and fluid characteristics. In this work, we utilize the modeling technique presented in [15], [16], where the total force of MR damper is separated into three parts: (i) Gas chamber

force, (ii) hydraulic force, and (iii) MR effect force as explained in chapter 2. A simplified schematic of a MR damper can be seen in Figure 3.1.

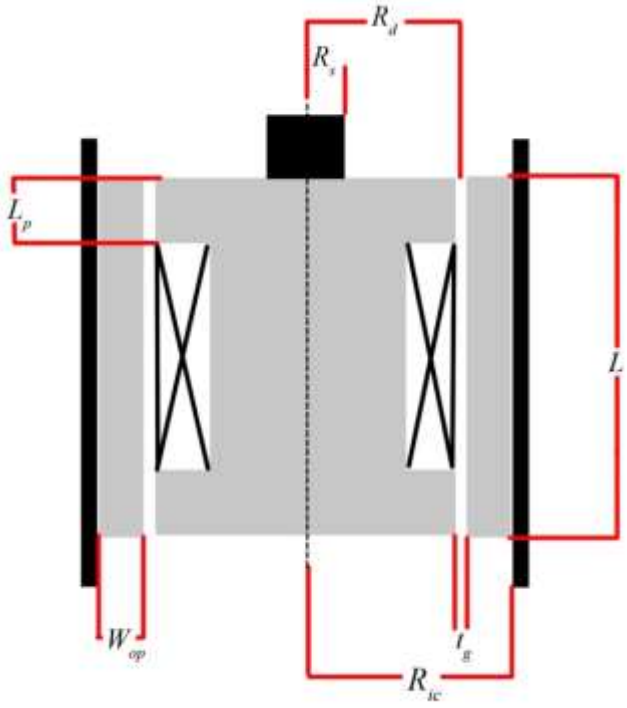

Figure 3.1 Schematic of a conventional MR damper piston.

For a given application, the main characteristics of an MR damper are the off state force, physical size, and maximum stroke as described in the following:

Off State Force: is equal to the sum of viscous force and force generated by the air chamber, normally when the magnetic circuit is not energized. The off-state force is the minimum damping force that can be obtained from the damper. The magnitude of this force is important from a reliability point of view. For example, when there is a loss of

magnetic field due to an electric failure this force should be large enough to safely operate the device. Also, the off-state force plays an important role in the performance of semi-active vibration control algorithms such as sky-hook. Thus for most applications the off-state force should be predetermined before the design is started.

Damper Size: Depending on the application, the damper size can be critical. For instance, in automotive applications the length and radius of the damper are determined by constraints such as the coupling mechanism, spring size, and the distance between the tire and chassis.

Maximum Stroke: The stroke of a damper is the total travel distance required for the mechanical system. Depending on the application the stroke magnitude can be as small as a few centimeters (e.g., in automotive/robotic applications) to a few meters (e.g., in large scale structural applications).

3.3. Design of MR Dampers

The quasi-static model presented in chapter 2 can be utilized to design an MR damper. To this end, there are certain considerations to be taken into account including manufacturing limitations, magnetic design of the MR piston, incorporating constraints, and the cost function.

Manufacturing limitations: In the design process of MR dampers, the manufacturing process is usually not taken into account. It should be noted that manufacturing limitations can have a significant effect on the design, manufacturability,

and the performance of the damper. In this work we incorporate limitations such as tolerances and standard pipe size in the design process to simplify the manufacturing stage. Machining tools such as lathe and mill machines have certain minimum tolerances. If these tolerances are taken into account in the design process; all the dimensions can be considered as discrete parameters instead of continuous ones. Parameter discretization can also be done by considering the standard raw material availability in the market. For example, when designing the cylinder of an MR damper, one may utilize off-the-shelf pipes with ANSI or ISO standard dimensions.

Magnetic Design of the MR piston: In designing MR dampers, one has to deal with a multi-domain magnetic structure with the objective of minimizing the losses and maximizing the magnetic field density in the MR fluid gap. In this respect, avoiding magnetic saturation is necessary since it can limit the magnetic flux in the circuit and cause magnetic losses. Magnetic bottlenecks can be avoided by adjusting the cross sectional areas of the magnetic circuit. Based on the magnetic flux conservation law (*KφL*), we can relate the cross sectional area of each part of the magnetic circuit to other parts as follows:

$$\Phi_1 = \Phi_2 = \ldots = \Phi_n \tag{3.1}$$

$$A_1 B_1 = A_2 B_2 = \ldots = A_n B_n \tag{3.2}$$

where Φ_i is the magnetic flux, A_i is the cross sectional area in each part of the circuit, and B_i is the magnetic flux density in each part of the magnetic circuit.

An operating point has to be selected when designing a magnetic structure based on the KφL rule. In this study, it is assumed that the device is operated at the edge of saturation. This means that all and every part in the magnetic structure, regardless of the

material, is at the edge of saturation. If two or more materials are used in the magnetic structure, the saturation magnetic flux density of each material can be considered as the operating point for that specific material to calculate the corresponding cross sectional areas. We refer to the above approach as *Area Equality*.

MR damper Model simplification: As discussed in chapter 2, the total force of an MR damper can be separated into gas chamber, hydraulic part, and MR part. There are five variables in formula (2.2); namely L, F_{vis}, R_d, t_g and A_p. The value of L is obtained depending on the application and space limitations as discussed earlier. The value for F_{vis} can also be found based on the off-state force (F_{min}) requirements. The cross sectional area A_p can be written in terms of R_d and t_g as follows:

$$A_p = (\pi R_{ic}^2) - (\pi (R_d + \frac{t_g}{2})^2 + (\pi (R_d - \frac{t_g}{2}))^2 \quad (3.3)$$

Substituting (3.3) into (2.2) and simplifying results in

$$R_d = \frac{12\dot{x}_p \eta L \pi}{t_g{}^3 F_{min}} \left(4 t_g{}^2 R_d{}^2 + R_{ic}^4 + R_s^4 - 2R_{ic}^2 R_s^2\right) \quad (3.4)$$

Simplifying (3.4), the following second order equation can be obtained in terms of R_d

$$\frac{12\dot{x}_p \eta L \pi}{t_g F_{min}} \; R_d^2 - R_d - \frac{(R_{ic}^4 + R_s^4 - 2R_{ic}^2 R_s^2)(12\dot{x}_p \eta L \pi)}{t_g^3 F_{min}} = 0 \quad (3.5)$$

For a specific t_g, the value for R_d can be calculated by solving (3.5).

There are five variables in (2.3), namely FMR, L_P, t_g, τ_y and A_p, that have to be determined. The term F_{MR}, also known as MR effect, should be maximized. The value for

A_P can be calculated using (3.2) and (3.5). The term τ_y is a function of the magnetic field strength over the magnetic poles in the annular duct which can be found using FEA. The relationship between τ_y and magnetic field strength for the LORD MR Fluid 132-DG can be found in Figure 2.8.The term τ_y can be represented using a second order equation as follows

$$\tau_y = C_0 + C_1 H_{MR} + C_2 H_{MR}^2 \quad (3.6)$$

$$C_0 = -1.457,\ C_1 = 0.3834,\ C_2 = -7.405\ e\text{-}4$$

Utilizing fundamental magnetism rules we have

$$H_{MR} = \frac{B}{\mu} \quad (3.7)$$

$$B_{MR} = \frac{\varphi}{A} \quad (3.8)$$

where A is the cross sectional area of the magnetic pole, H is magnetic field strength, B is the magnetic field density, and μ is the magnetic permeability of MR fluid. Since the fluid flow gap is an annular duct, the cross sectional area is not constant through the duct. Thus the average value is obtained by integrating the magnetic field density as follows:

$$B_{MR} = \frac{1}{t_g}\int_{R_d-\frac{t_g}{2}}^{R_d+\frac{t_g}{2}} \frac{\varphi}{L_p 2\pi r}\, dr = \frac{\varphi}{t_g L_p 2\pi}\left[\!\left[\ln\right]\!\right]\left(R_d + \frac{t_g}{2}\right) - \ln\left(R_d - \frac{t_g}{2}\right)\Big) \quad (3.9)$$

This formula can be further simplified as follows:

$$B_{MR} = \frac{\alpha}{t_g L_p} \quad (3.10)$$

where α is a constant value given by $\alpha = \frac{\varphi}{2\pi} \left(\ln\left(R_d + \frac{t_g}{2}\right) - \ln\left(R_d - \frac{t_g}{2}\right)\right)$.

Using (3.11) we can calculate the value of HMR as follows:

$$H_{MR} = \frac{B_{MR}}{\mu} \quad (3.11)$$

Since the system is operating near its saturation point, it can be assumed that the MR fluid acts in its linear region with the value of μ being constant. Hence,

$$H_{MR} = \frac{\alpha}{t_g L_p \mu} = \frac{\alpha'}{t_g L_p} \qquad \alpha' = \frac{\alpha}{\mu} \quad (3.12)$$

By substituting (3.12) and (3.6) into (2.3) we have,

$$F_{MR} = \left(A_p - A_s\right) 2 \frac{c\, L_p}{t_g} \left(C_0 + C_1 H_{MR} + C_2 H_{MR}^2\right) \quad (3.13)$$

Assuming that the only unknown in (3.13) is L_p, we can find it by differentiating (3.13) and maximizing F_{MR}, i.e.,

$$\frac{d\, F_{MR}}{d\, L_p} = \left(A_p - A_s\right) 2\, c \left(\frac{C_0 t_g^2 L_p^2 - C_2 \alpha'^2}{t_g^3 L_p^2}\right) = 0 \quad (3.14)$$

Hence

$$C_0 t_g^2 L_p^2 - C_2 \alpha'^2 = 0 \quad (3.15)$$

Since L_p is not zero, (3.15) can be simplified as follows

$$C_0 t_g^2 L_p^2 = C_2 \alpha'^2 \quad (3.16)$$

From which we have

$$L_p = \sqrt{\frac{C_2 \alpha'^2}{C_0 t_g^2}} \tag{3.17}$$

The above formula can be used to find the optimum value for magnetic pole length. As an alternative the value of L_p can be determined by considering all and every feasible values for L_p between zero and half of entire length of the piston.

3.4. Optimal Design

In this section, the results obtained in sections 2 and 3 are used to introduce a comprehensive approach in the optimal design of MR dampers with the objective to maximize the MR effect force, also known as dynamic range. This approach is developed based on the quasi-static model for valve mode MR dampers; however, the same approach can be used for other types of MR dampers.

As a baseline for this study the FOX DHX RC4 is used, which is a commercial adjustable damper. The goal is to design an MR piston with integrated AlNiCo as the core which can be retrofitted in the DHX RC4 with the specifications and constraints given in Table 2. The machining tolerance was set to 0.01 mm which is the finest accuracy achievable with common machining tools. The off-state force in this case was set to match the minimum compression force achievable from the DHX RC4 at a speed of 0.25 cm/s.

Table 3.1 Design specifications and constraints.

Parameter	Value
Machining tolerance	0.01 mm
Length of the piston (*L*)	20 mm
Off-state viscous force (F_{min})	100 N
Cylinder inner radius (R_{ic})	13.3 mm
Shaft radius (R_s)	8 mm
Radius of Core (R_c)	7.93 mm

The optimization steps are as follows:

Thickness of gap (t_g): Given the machining tolerance in Table 3.2, a vector of all possible values for the thickness of fluid flow gap (t_g) is generated between 0.2mm to 1.5mm. This will result in a vector of 130 feasible values for t_g. This range is considered to be large enough to cover all feasible solutions.

Average radius of fluid flow gap (R_d)*:* The elements of the vector obtained in the last step will be used to calculate values for R_d using (3.2) and the off-state force. At this stage we have to make sure that all of the values found for R_d by solving (3.2) are positive and real.

Width of the outer piston (W_{op}): Given the inner radius of cylinder, t_g, and R_d, the value of W_{op} can be obtained as follows

$$W_{op} = R_{ic} - (R_d + \frac{t_g}{2}) \quad (3.18)$$

Alternatively, when the radius of the core is known, the value of W_{op} should be calculated using the *Area Equality* approach when the radius of the core is known. This can be done using equation (3.19). The material of the core is AlNiCo while the outer pole is made of steel 1018. The saturation point for steel is 1.8T and for AlNiCo5 is 1.2T. Thus using the Area Equality rule we have

$$\pi R_c^2 = \frac{1.2}{1.8} \left((\pi R_{ic}^2) - (\pi (R_{ic}-W_{op})^2)\right) \quad (3.19)$$

This would be useful in the cases that off the shelf ANSI or ISO standard AlNiCo alloy bars are being used. In this case we used a standard AlNiCO bar with radius of 7.93mm (5/8 inch).

Core radius (R_c): In this specific case the radius of the core is known because of using standard AlNiCo alloy bars however if the core radius is unknown this approach can be taken. Using the *Area Equality* rule, the radius of the magnetic core can be found. The equation (3.19) is useful in this case as well.

Length of magnetic pole (L_p) : Since in each solution vector we have the value of t_g and R_d, we can use (3.20) to find the value of L_p. Alternatively, the values for L_p can be calculated using an approach similar to what was done for t_g by considering a vector of all feasible L_ps. In this case, the minimum value for L_p should be calculated using area equality rule to make sure we avoid magnetic saturation in the poles. The minimum value for L_p can be calculated using the following formula.

$$Lp_{\,min} = \frac{\pi(R_{ic}^2 - \left(R_d + \frac{t_g}{2}\right)^2)}{2\pi(R_{ic} - W_{op} - t_g)} \quad (3.20)$$

In this study, the above method was used to ensure that every single feasible solution is taken into account.

FEA analysis: At this stage we have a vector of all feasible solutions for the MR damper design problem. These solutions should be analyzed using FEA in order to find the optimum solution. To this end, we utilized COMSOL and Matlab Livelink packages to find the MR forces for each of the calculated vectors of solution. The results are illustrated in Fig 3.2. The wire gauge was selected as AWG28 and the number of windings was set to maximum, considering the area available for coil in each design.

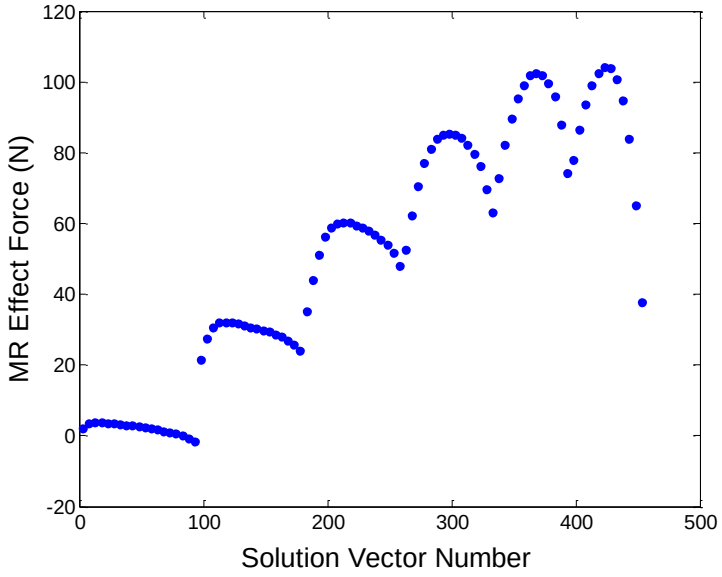

Figure 3.2 The simulation result for calculated MR effect force for all the feasible solutions.

The optimum solution is the vector number 431 with MR force of 108N. As it can be seen in Fig. 3.2, there are many extrema points. However, using the proposed method the global optimum solution can be found since we have taken all of the feasible solutions into account and none of the feasible data point has been missed. The FEA analysis results for the optimum design are shown in Fig. 3.3. The overall time to perform the above

optimization process was 22 minutes on a standard desktop computer with 16GB of RAM with an Intel Core i7 4470 CPU.

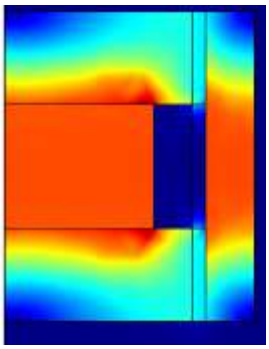

Figure 3.3 Axisymmetric FEA results for the optimum MR piston.

The values found using this optimal design approach can be found in Table 3.3. The dynamic range of 108N is a reasonable value for such a small MR damper which is comparable to the dimensions and dynamic ranges reported in the literature (see e.g., [44]–[46] . Considering the results of section 2.4 that verified the accuracy of quasi-static model and the fact that all and every feasible solution has been taken in this design process the result presented in Table 3.2 is the optimum solution.

Table 3.2 Optimal Design and simulation results.

Parameter	Value
t_g	0.73 mm
W_{op}	2.61 mm
L_p	6.00 mm
MR Force obtained from simulation	108 N
Off-state viscous force obtained from simulation	100 N

3.5. Fabrication and Experimental Results

Based on the results obtained in section 4, an MR piston with AlNiCo core was built. The parts were made of Iron 1018 with a machining tolerance of 0.01mm (10 micron). The parts of the MR damper are shown in Fig. 3.4.

Figure 3.4 Fabricated MR damper parts based on the optimal design approach.

The electromagnet was built using 180 turns of AWG28 wires around the AlNiCo core and the piston was retrofitted in a commercial Fox RC4 damper. The damper was tested using a Roehrig shaker system as shown in Fig. 3.5. This shaker is able to generate sinusoidal displacements with maximum amplitude of 2.54cm (1 inch) and adjustable frequency (speed).

Figure 3.5 Designed damper under test using a Roehrig shaker.

The test was performed at 37.7^{o} C with a gas chamber pressure of 100Psi using a sinusoidal excitation with a maximum speed of 25 cm/s. During the test, the sealing drag force was measured and subtracted from the results. The experimental results were

obtained while the AlNiCo was fully magnetized and demagnetized. Fig. 3.6 illustrates the force-velocity curve for the experiments.

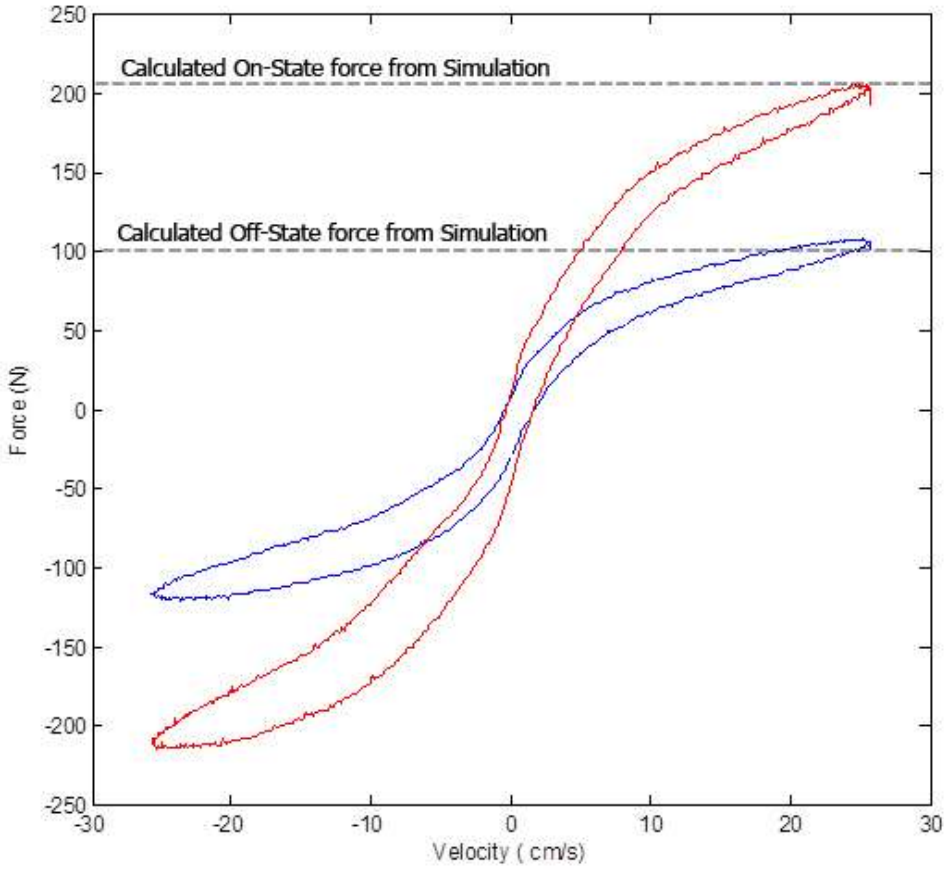

Figure 3.6 Experimental results for on-state (red) and off-state (blue) AlNiCo states and comparison with simulation results.

As it can be seen in Fig. 3.6, the curves exhibit hysteresis shaped loops. In order to magnetize the AlNiCo core, the coil was excited with a 100ms pulse of 7A current and for demagnetizing purpose the same current was applied in the reverse direction for 24ms. When the AlNiCo is magnetized (on-State), the MR fluid is activated and thus the fluid flow through the piston requires more pressure which leads to higher forces. On the other hand, when the AlNiCo is demagnetized (off-State), the fluid can flow easily through the piston with only the hydraulic force being in effect. As a result, smaller forces are obtained. The maximum force in the off-state is about 110N, considering that the gas chamber force has

been removed from the results by the measurement system. In the on-state, the max force reaches 213N, which means that the MR force is about 103N. The error does not reach more than 4 percent comparing to the simulation obtained using the quasi-static model. The above results can be attributed to the relatively high speed of the tests performed and possible fabrication errors such as piston and rod misalignment. Therefore, the experimental results match simulation values with negligible error.

3.6. Conclusion

MR dampers have a complex behaviour that makes their design and optimization quite challenging. The optimal design method presented in this paper can be utilized in multi-material structures with guaranteed convergence to the global optimum solution with a reasonable amount of computational effort. A particular feature of the proposed design approach is that fabrication limitations can be taken into account. Thus the approach leads to the reduction of the computational complexity and achieving feasible solutions. The proposed method was used to design and manufacture a valve-mode MR damper with integrated AlNiCo as the core. The designed damper prototype was manufactured and tested experimentally. The experimental results were compared with theoretical results obtained in the design stage which validates the efficacy of the approach in finding the optimum solution.

Chapter 4. Alternative Configurations for Low-Energy, Low-Mass MR Dampers

4.1. Introduction

In pursue of low-energy, light-mass MR dampers solutions to optimally design conventional MR dampers have been investigated. As it was concluded from outcome the previous chapters, enhancing the performance and reducing the weight of MR damper is challenging and more or less impossible using the conventional configuration for MR dampers. While optimal design approaches are slightly helpful in minimizing the weight and energy consumption of MR dampers, they cannot rectify the issues and barriers against the development of MR technology. Investigation of alternative configurations is necessary to overcome the drawbacks of MR dampers. For this purpose a deeper insight into the mechanism of MR damper is essential. In this chapter the operation of MR dampers will be studied in more detail and alternative configurations will be proposed with the objective to maximize the use of the entire length of the damper while minimizing the energy requirements by employing AlNiCo as the core of the damper.

4.2. Strategies to Increase Dynamic Range and Decrease the Weight of MR Dampers

As a fundamental fact, having two MR dampers with similar size and weight but different configuration, if one of those MR dampers offers a larger effective dynamic range (F_{MR}), compared to the other one, it can be used to decrease the overall size and mass. Let's say if a novel configuration is compared with a conventional MR damper, called I-piston in this context, with similar off-state force, weight and size. If the novel configuration

offers a wider dynamic range; that can be utilized to design lighter MR dampers. This happens by designing the off-state force and dynamic range to match the one for conventional dampers while the cylinder diameter is decreased. Thus our mission is to identify alternative configurations that can increase F_{MR} or the effective dynamic range of the damper as much as possible.

One of the major ideas to improve the performance of MR dampers is to increase the effective length of the magnetic poles (L_p). This idea has been investigated in [16], [47] by employing multi-coil MR dampers. The idea of multi-coil MR dampers can be expressed as putting two I-pistons in series. Doing so will increase the dynamic range ratio. However, the off-state force needs to be recalculated because the length of the piston (L) has changed.

Multi-coil design is a great method to increase the dynamic range in a fixed cylinder diameter. However, it doesn't help mass reduction since the length of the damper and the piston mass are increased by adding a new part to the piston. This design can be classified in the same category as I-piston.

The idea of increasing L_p was investigated in [48], [49] by employing a vertical coil structure. The highlight of this configuration is that almost the whole length of the piston is used as the magnetic pole except the top and bottom parts that are used as an area for the coil to be wound. In this method, not only a higher length of the piston is used as the magnetic pole but also no extra part is added to the piston, therefore, the weight is not affected much when compared to the I-piston design.

Another idea for increasing L_p is to modify the I-piston design so that the coil area, which has no usage from the magnetic point of view, is also utilized as an effective magnetic pole. This idea is the baseline for a novel configuration concept that I refer to it

as Zebra. In this design, the electromagnetic coil is covered with a set of inner poles and the outer pole is cut into smaller sections. The inner and outer poles are isolated with insulators made of non-magnetic materials such as Aluminium or plastic. These magnetic insulations guide the magnetic flux through the annular duct. By utilizing this method, the whole length of the piston, except the magnetic insulation parts, will be used as an active magnetic pole. A schematic of the Zebra concept is shown in Figure 4.1.

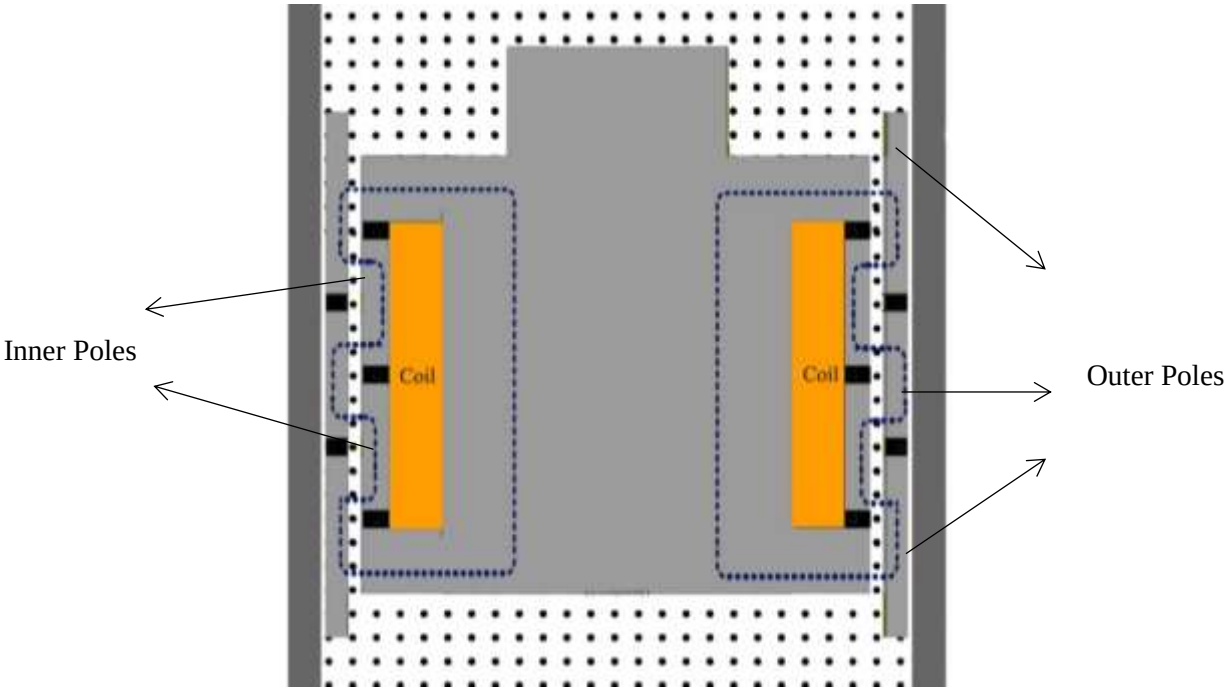

Figure 4.1 Diagram of the Zebra concept.

So far, three design concepts have been introduced. In order to compare the performance of these concepts, a standard design and test condition should be defined. For this purpose, some limitation and specification were defined and summarize in Table 4.1.

Table 4.1 Design assumptions.

Parameter	Value
Off state force at 25 cm/s velocity	200 N
Length of piston	20 mm
Cylinder inner diamater	28.57 mm (1.125Inch)
MR fluid type	Lord 132DG

Given the design criteria from Table 4.2, the three design concepts were modeled using COMSOL Multiphysics. In this study, the I-piston design was optimally designed to achieve an off-state force of 200 N with the largest dynamic range possible. The other two designs were also modeled by using the same dimensions which are not necessarily optimal. The results of the Finite Element Analysis (FEA) can be seen in Figure 4.2.

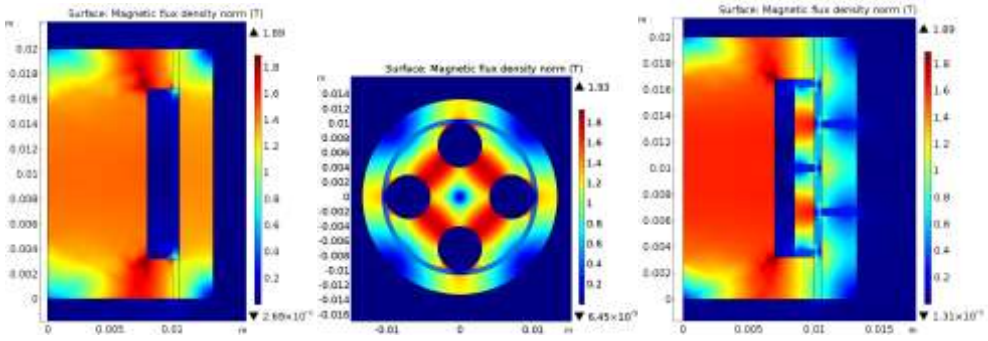

Figure 4.2 Illustration of I-piston side view (left) vertical coil top view (center) and Zebra side view (right) and their FEA analysis

Comparing the results of the FEA simulation the following results were obtained:

Table 4.2 Alterntive configurations comparison.

Design Concept	Off state force at 25 cm/s (N)	Active pole length (mm)	Field density average in the duct (T)	Calculated MR force
I-Piston	200	12.8	0.477	65
Vertical coil	200	16	0.433	72
Zebra	200	17.5	0.617	128

It can be seen in Table 4.2 that the vertical coil design and the Zebra design have significantly higher MR forces compared to the I-piston design. Thus, if the Zebra or vertical coil configurations are used for designing an MR damper, the damper mass can be decreased. Since our aim is to design MR dampers for mass and energy sensitive applications, each of these designs should also be studied from the energy consumption point of view.

4.3. Integrating AlNiCo into MR Damper Configuration

Designing an MR damper with AlNiCo is quite similar to the common MR damper design methods. However, one should take into account the magnetic characteristics of AlNiCo. AlNiCo is a type of permanent magnet that has a relatively low coercivity compared to other types of permanent magnets, such as rare-earth magnets, while it has a reasonable remanence or magnetic strength. The most common type of AlNiCo for controllable magnets is AlNiCo5 that has an anisotropic crystal structure. This type of magnet can only be magnetized in one orientation [50]. Thus, AlNiCo is not compatible with MR damper concepts that require the magnet to be magnetized in different orientations. More specifically, the vertical coil concept is not compatible with AlNiCo 5. Zebra concept requires magnetization in one direction that makes utilization of AlNiCo core possible in this concept.

To verify the performance of Zebra design compared to the I-piston configuration, an experimental validation should be performed. For this purpose, the DHX RC4 commercial shock absorber made by FOX Inc. was chosen as a baseline and the Zebra and I-piston configurations were designed to fit into the DHX RC4 frame. AlNiCo5 model was imported into the design process to optimally design the I-piston and Zebra concepts powered by AlNiCo. The main constraint in the optimal design process was to avoid

magnetic saturation while the MR effect was maximized. Also, the off-state force at a speed of 25cm/s was set to 200N and was considered as a constraint in the optimal design process. The FEA results for the Zebra concept can be seen in Figure 4.3. In this figure, it can be seen that the AlNiCo inner poles and outer poles are all on the edge of saturation. It is worth mentioning that the saturation point is about 1.2T for AlNiCo and 1.8T for Iron 1018 that were used to design the magnetic parts of the structure.

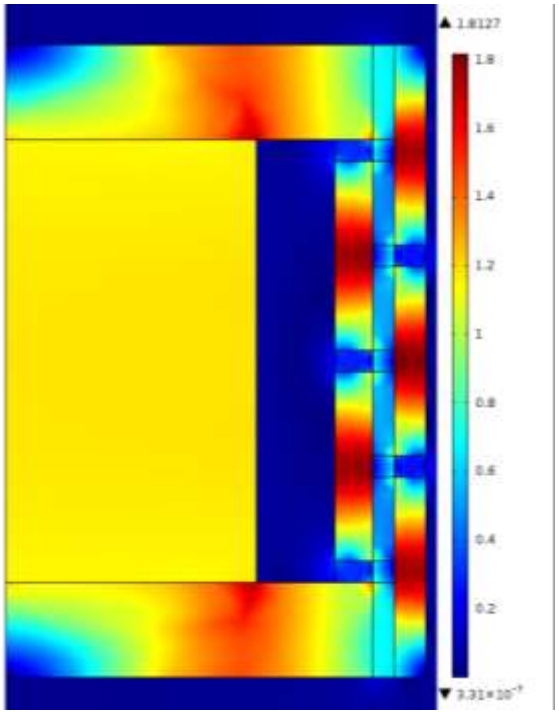

Figure 4.3 FEM result of optimally designed AlNiCo5 powered Zebra design.

The same study was also conducted for an I-piston MR damper. The damper was optimally designed to be used as a reference design for comparison with the Zebra design. The I-piston design can be seen in Figure 4.4.

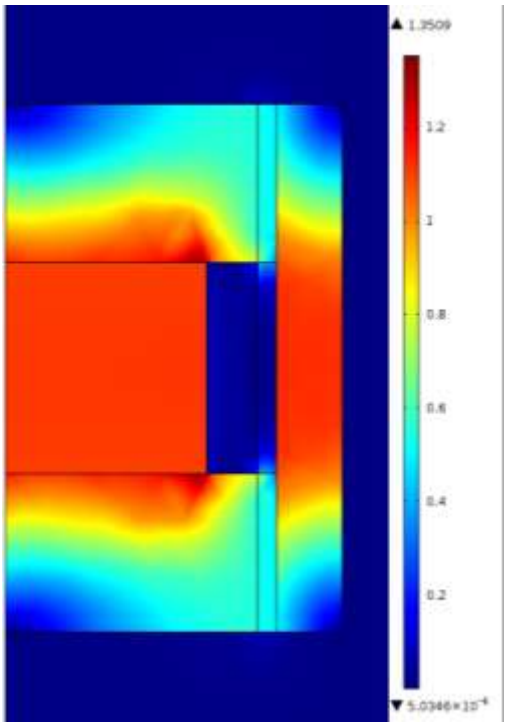

Figure 4.4 FEM result for optimally designed AlNiCo5 powered I-piston design

4.4. Fabrication and Experimental results

The results of the FEA analysis were used to manufacture two MR dampers by using the DHX RC4 as a baseline for the design. The manufactured dampers can be seen in Figure 4.5.

Figure 4.5 Designed prototypes of the Zebra and I-piston concept.

The dampers were wired with AWG-28 wires. Each of the pistons was wrapped in a Teflon strip to make sure all the fluid goes through the annular duct and it does not bypass the valve. Finally, the dampers were filled with Lord MRF 132DG and all the air was bled out of the cylinder. To avoid the cavitation and compensate the volume change due to the damper rod volume, the gas chambers were utilized and their pressure was adjusted to 100Psi.

A Roehrig shaker was used for testing the dampers and measuring their performance. The test scenario used is as follows:

1. Preheat the damper to 32.2^{o}C (90^{o} F).
2. Measure the seal drag and gas chamber force
3. Shake the damper with sinusoidal input with max speed 25cm/s and amplitude of 2.54 cm (1 inch).
4. Remove the seal drag and gas chamber force

The test was done both on the Zebra piston and the I-piston in the off-state and on-state modes and the dynamic ranges were observed. The obtained result for the I-piston can be observed in Figure 7. The dampers were switched between the on and off state using a power electronic circuitry that let us adjust the voltage and time duration of the electric pulses. The amount of energy used for switching the dampers between the two states was roughly about 6 J which means 60 W of power for a period of 100ms. Obviously, the electrical behavior of the MR damper is inductive-resistive that causes the electric current and voltage relations to seem similar to a first order system.

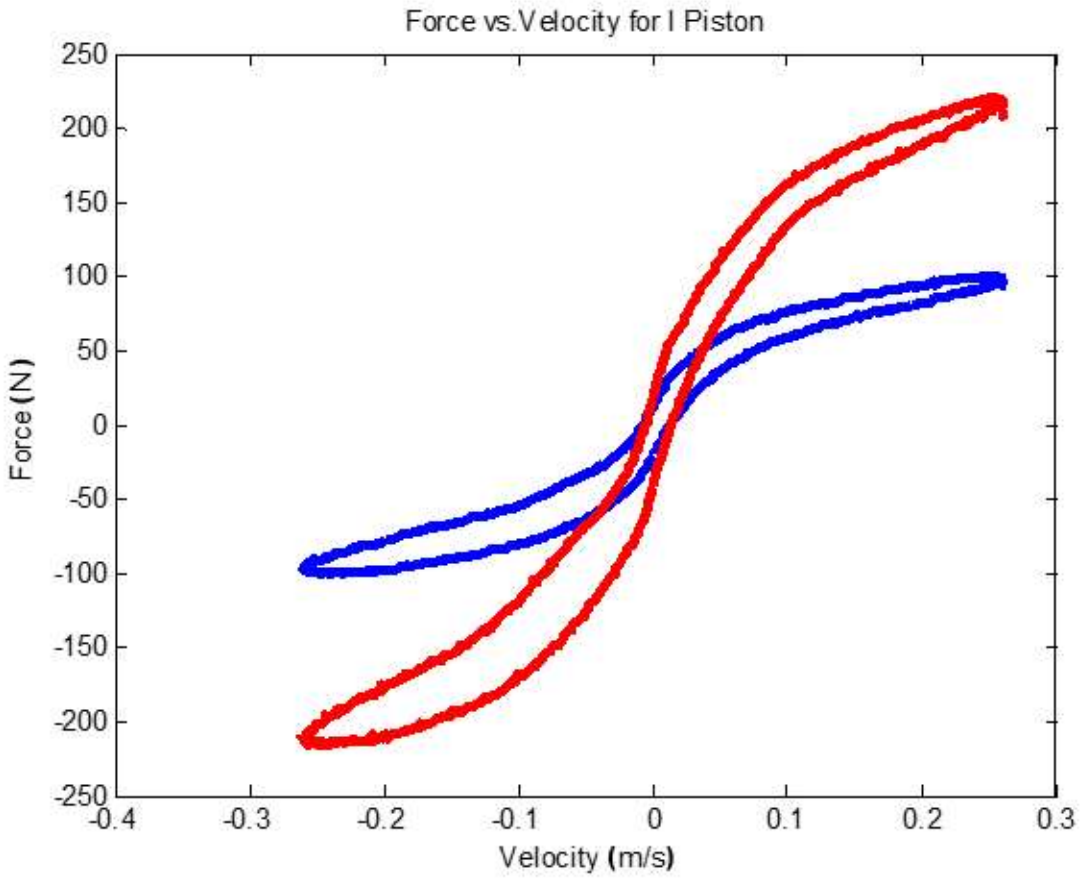

Figure 4.6 Experimental results for off-state (red) and fully on-state (blue) of the I-piston configuration.

As it can be seen in Figure 4.6, the off-state force is 110N and the MR effect force is about 103 N. The amount of MR effect force is quite small which is due to the relatively small diameter of the damper that leads to the smaller surface of contact for the magnetic poles. This is one of the drawbacks for MR dampers that have limited their application. The results presented here differ from the simulation results presented in Table 4.2. This is mainly because in the above design AlNiCo was integrated into the core of the damper. AlNiCo saturates at a lower magnetic field density that results in lower magnetic flux generated in the core hence the less MR effect force in the AlNiCo MR damper can be justified.

Figure 4.7 represents the results for the Zebra configuration.

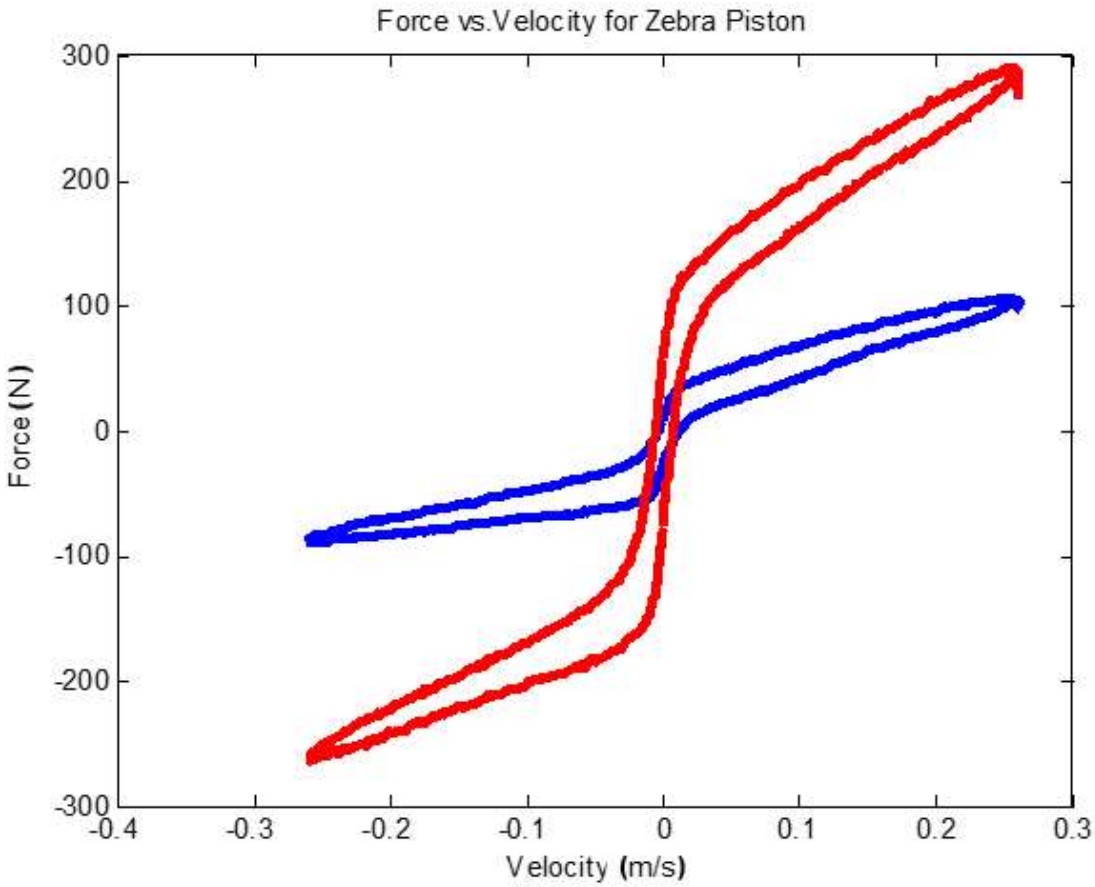

Figure 4.7 Experimental results for off-state (red) and fully on-state (blue) of the Zebra piston configuration.

The off-state force for the built Zebra piston is measured to be 108N, which slightly differs from calculations due to manufacturing errors. The maximum on-state force was recorded as 296N. The Zebra piston tested here has similar dimensions and mass to the I-piston damper. While the off-state forces for the two dampers are very close, the Zebra configuration is able to provide significantly higher dynamic range (~ 1.8 times) because of the higher area of magnetic contact it has.

This experiment demonstrates superiority of the Zebra to the conventional MR dampers is thus verified. The proposed design has the ability to provide a larger dynamic

range that can considerably improve the performance of semi-active vibration control systems. The enhancement in the dynamic range makes this concept suitable for mass-sensitive applications. Finally, the proposed design is AlNiCo compatible, which means that it can operate on smaller and lighter batteries and power sources.

The AlNiCo powered MR dampers require a feasible and effective control strategy for operation. In the next section a novel strategy to effectively and efficiently control AlNiCo powered MR dampers will be proposed.

4.5. Control Strategy for AlNiCo Powered MR Dampers

The application of AlNiCo as a controllable magnet has been studied in several different applications such as robotics and electric machines [51]–[53]. The challenge in controlling the magnetic behavior in a permanent magnet is to overcome their hysteric behavior and harness them in an energy efficient way [54]. Although the industrial use of controllable PMs is increasing as an energy efficient solution, their control have not been investigated as deserved.

The objective of this section is to investigate the behaviour of AlNiCo magnets and propose an efficient control approach to switch AlNiCo from an arbitrary state to the desired operating point in order to be used in energy-efficient magnetic structures such as MR dampers, electric machines and magnetic switches.

4.5.1. Behavior of AlNiCo Magnets

The characteristics of a permanent magnet is usually represented with its saturation hysteresis curve. This curve can be represented with two main properties which are coercivity and remanence. These two parameters are the points that the hysteresis

curve of a permanent magnet crosses the axis on B-H curve of the magnet. For instance, the saturation B-H curve for a permanent magnet can be seen in Figure 4.8.

The higher coercivity means that it would be harder to demagnetize the magnet. In other words, coercivity tells how much magnetic field strength is required to demagnetize a permanent magnet. The parameter remanence defines how strong a permanent magnet can be. Remanence represents the magnetic field density of the magnet when no external factor such as a coil or another magnet is in effect.

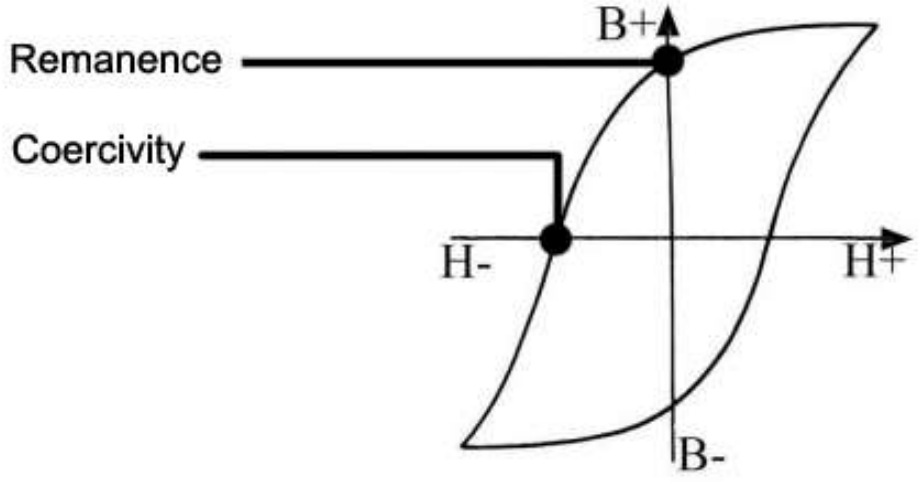

Figure 4.8 A saturation hysteresis curve for a permanent magnet.

Practically a magnetic material can be excited into any point within the saturation hysteresis loop by winding a coil around it and exciting the coil in order to generate enough magnetic field strength (H). Once the electric current is stopped, the magnetic field strength will become zero, and the magnetic field density will set to a constant.

The common method to present magnetization characteristics of a commercial magnet is to use its demagnetization curve. Demagnetization curve is a quarter of the saturation hysteresis curve that summarizes the characteristics of a commercial

permanent magnet in a concise way. The demagnetization curve for AlNiCo5 is depicted in Figure 4.9.

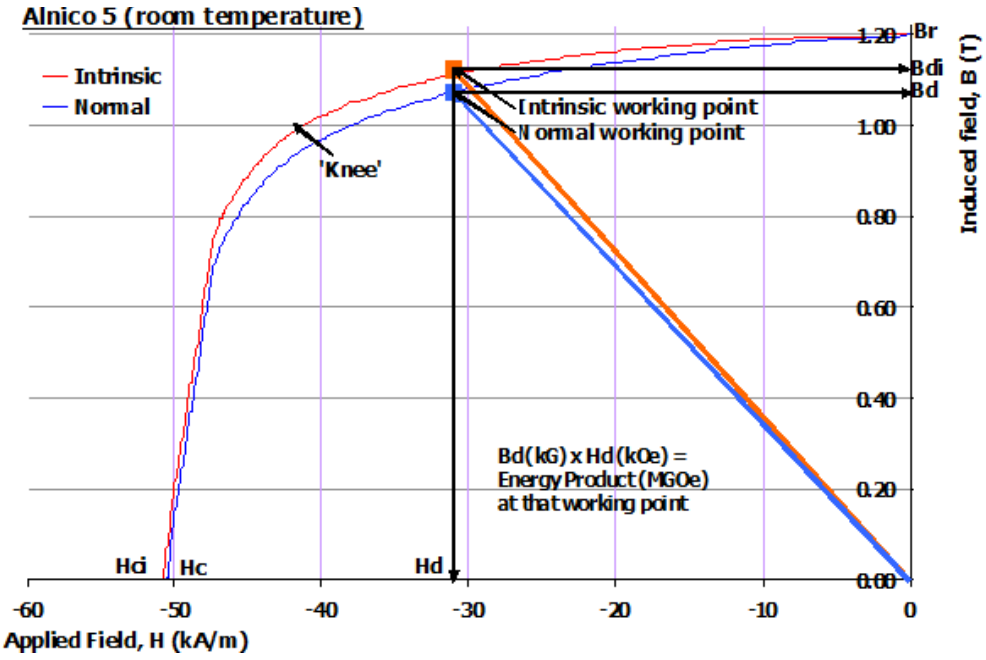

Figure 4.9 The demagnetization curve for AlNiCo5 [55]**.**

In order to use this characteristic curve for simulation purposes, it was digitized and an exponential curve was fit on it. Figure 4.10 show the fitted curve.

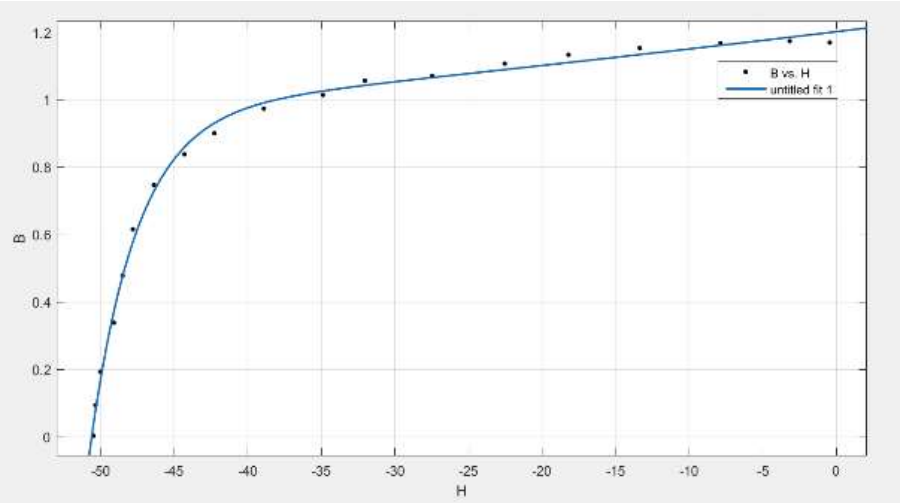

Figure 4.10 The fitted curve of the intrinsic demagnetization curve for AlNiCo5.

The equation for the fitted curve is:

$$H = 1.324\, e^{3.653\, B} - 46.47\, e^{-0.045\, B} \quad (4.1)$$

This formula can be used to relate the desired operation point (B) to its associated magnetic field strength (H) and using H the electric current can be calculated :

$$I = \frac{LH}{N} \quad (4.2)$$

4.5.2. Control Strategy for AlNiCo Magnets

The control of AlNiCo magnets due to their non-linear hysteric behavior is quite challenging. Although many efforts such as [56], [57] have been done to model hysteric systems, there is no efficient method to formulate the hysteric behavior of magnetic materials. One of the feasible ways to control AlNiCo is to excite it into its saturation point and then control it from the saturation point to any desired value. The AlNiCo can be excited into saturation with any magnetic field strength higher than 50 KA/m. The advantage of such strategy is simplifying the hysteric system into a linear resistor-inductor (RL) model.

RL load can be easily modeled by a first order system with the following transfer function and state space representation.

$$\frac{I}{V} = \frac{1}{R+LS} \quad (4.3)$$

$$\dot{X} = \dot{I} = -\frac{R}{L} I + \frac{V}{L} \quad (4.4)$$

$$Y = X \quad (4.5)$$

This model, while combined with formulas (4.1) and (4.2), can be used to simulate and control an AlNiCo magnet based on the strategy explained. Another advantage of this approach is its compatibility with different types of control such as PI and Model Predictive Control (MPC).

4.6. Conclusion

In this chapter, different aspects of MR damper design and manufacturing were studied to explore new possibilities to improve the mass and energy consumption. Different configurations and strategies were presented and a new design concept was proposed that can improve the dynamic range and significantly decrease the mass of MR dampers. It was shown that the proposed concept, Zebra, is able to maximize the length of the magnetic pole and the effective magnetic surface; hence improving the dynamic range and MR-effect force.

Furthermore, different strategies to minimize energy consumption in MR dampers were investigated and AlNiCo as a controllable magnetic latch was introduced. It was shown that Zebra concept is compatible with AlNiCo so that it can be used to design and build low-power MR dampers.

Next, a Zebra MR Damper and a conventional MR damper were optimally designed and built with an integrated AlNiCo core. The initial design in last section was done with the purpose of comparing the performance in was not necessarily the optimal solution. In this section both the Zebra and I-piston concepts were optimally designed with AlNiCo core to assure the best results. The two dampers were tested under standard conditions and it was shown that the Zebra concept has significantly better performance in terms of MR effect force and energy consumption when compared to conventional dampers. It is concluded that the Zebra concept has a great potential to improve the

performance of semi-active suspension systems while minimizing their mass and energy consumption.

The behavior of AlNiCo magnets was studied in more detail and a feasible and effective control strategy was proposed for AlNiCo magnets.

Chapter 5. MR Dampers with Asymmetric Damping Behavior

5.1. Introduction

The conventional MR dampers are mostly designed to provide symmetric damping characteristics in compression and rebound half cycles. This makes their utilization impossible or quite expensive in terms of energy consumption wherever different damping force is required in compression and rebound. For instance, in mountain bikes, the shock absorbers are usually tuned in a way to have less damping force in compression and higher force in the rebound half cycle so that riders have a smoother ride [58]. This is the same in many other applications such as automotive suspension systems [59]–[61]. In [62] it is suggested to use the MR effect and switch between magnetic states in compression and rebound to achieve asymmetric damping characteristics. The rebound force required in such applications is usually 3 to 5 times higher than the compression force [63], which is not achievable by MR effect in most cases. The amount of the force generated by the MR effect in MR dampers highly depends on the active area of magnetic contact and the magnetic field the coil can generate. Wherever the size and weight of the damper is a concern, the size and dimensions decrease and as a result, smaller coil and less active magnetic area of contact will be available, this leads to a smaller MR effect force. Moreover, when weight is a concern, there would be less room for the batteries. For instance, in portable systems such as bikes, prosthetics and robotics low energy consumption is a necessity to decrease the weight of the entire system and improve the lifetime of the battery. In the light of these, the MR effect is not the best way to generate asymmetric damping characteristics and alternative methods should be investigated.

Mountain bike manufacturing industry is one of dynamic and rapidly growing sectors that have developed significantly in the past couple decades as more consumer have shown interest in using them for athletic and recreational purposes. Several studies have been done on the dynamics and design of mountain bikes such as [58], [64]–[66] several of which have been done to study the suspension systems and specifically dampers [65], [67], [68],[69] and [70]. Although extensive research has been done on the design of bike suspension systems, application of MR technology has not been very well studied in this field and only a limited number of investigations have been done [71]–[73]. The challenges in applying MR technology in bike industry are high weight, high energy requirements, heat control, and the necessity of asymmetric damping behavior.

In this study we seek to address the challenges of applying MR technology in mountain bike industry to minimize the weight, energy consumption and excess heat generation while providing asymmetric damping characteristics. Similar to the design approach in chapter 4, DHX RC4 is considered as a baseline for the design and the objective is to design an MR damper that can match the characteristics of this commercial damper.

5.2. Damping Mechanisms

In order to design an MR damper with asymmetric behavior, different methods of generating damping force in hydraulic dampers should be investigated. The common methods in damping force generation can be categorized into three different groups.

5.2.1. Flow Restriction and Rectification Using Shim Stacks

Shim stack is a common method to adjust the characteristics of hydraulic dampers. The most outstanding feature of shim stacks is their ability to rectify the fluid flow direction and apply the force in one direction that can be compression or rebound. For instance, the operation of a piston equipped with shim stacks can be seen in Fig 5.1.

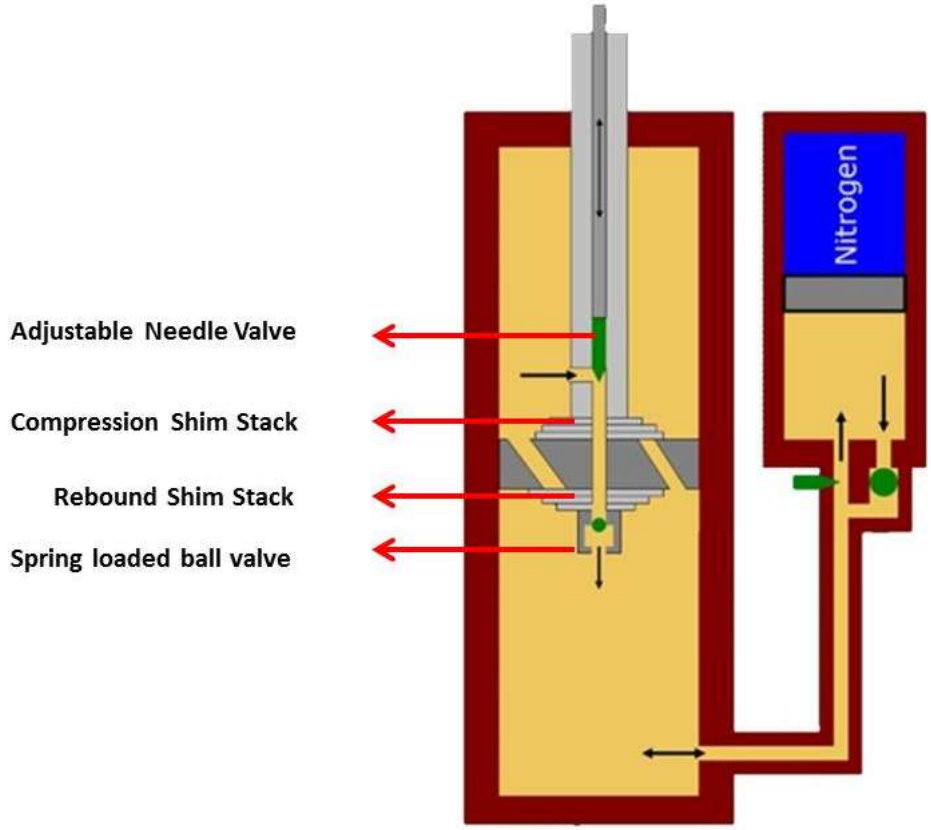

Figure 5.1 The schematic diagram of a conventional hydraulic damper with different passive valve mechanisms.

There are two shim stacks depicted in Fig 5.1 each of those is activated in one half cycle. The quantity, thickness and material of shims can be adjusted to achieve certain characteristics and damping force.

5.2.2. Adjustable Needles and Spring Loaded Ball Valves

The other common method to adjust the damping force in hydraulic dampers is using adjustable needles and spring loaded ball valves. This method is used wherever wider range of force or full blockade is required. The needle can be used to adjust the fluid flow in a wide range by opening and closing an orifice that fluid flows through. The spring loaded ball valve is also an automated mechanism to rectify the fluid flow. Fig 5.1 depicts the schematic of an adjustable needle and spring loaded ball valve.

5.2.3. MagnetoRheological (MR) Effect

There are two types of smart fluids known with viscosity adjustability used for shock absorption; ER fluid and MR fluid. These fluids are made by dispersing micron and nano-sized particles in a carrier fluid. While the ER fluid offers the higher stability of the particles, the MR have much better performance and have been more widely used in commercial products. In this method, the hydraulic fluid within the damper is altered with a smart fluid with adjustable viscosity and the fluid is excited with magnetic field for MR fluids and electric field for ER fluid. In this study, we focus on MR dampers as their superiority has been proven in several prior works [13], [74].

5.2.4. Comparison of Mechanism

The downside of using shim stacks and adjustable needles for generating asymmetric behavior is the fact that adjusting the tuning in real time can be very challenging if not impossible. There have been some efforts to automate mechanical valves to be adjustable electronically by using solenoid valves and electromotors [75], [76]

however due to the complexity, costs of maintenance and high response time they have not been very well received.

Damper adjustability is more sought on the compression side while the rebound force of the damper is tuned very less often. Considering the aforementioned facts the most feasible solution to achieve an adjustable damper is to combine the mechanical valves with the MR technology. On one hand, it has been mentioned that the required rebound forces are higher in comparison to compression force while this force less often is tuned. On the other hand, the compression force is relatively smaller and easily achievable by MR technology. Also the compression force is the force that regularly needs to be adjusted depending on the situation and riders' preference. Thus, the aim in this research is to design a hydraulic damper based on MR technology that utilizes MR effect to tune the compression force while taking advantage of conventional hydraulic valves to generate the rebound force and provide the sophisticated functionalities required for a hydraulic damper.

5.3. Designing the Asymmetric Damper

As mentioned in section 5.1 the aim of this design problem is to achieve the characteristics of a DHX RC4 damper by employing MR technology. DHX RC4 is a commercial damper for downhill mountain bikes that have adjustable mechanical valves for tuning the compression and rebound force. This damper also utilizes shim stacks on compression and rebound circuits. For a downhill rider it is essential to be able to switch and adjust the compression circuit between locked and open to optimize the ride and minimize the unnecessary damping. For this purpose and in order to measure the force range that a DHX RC4 damper can provide; several tests and characterisation was done. Fig 5.2 demonstrates the force-displacement curves of this damper in locked and open

states for a sinusoidal excitation with an amplitude of 2.54 cm and maximum velocity of 0.25 m/s.

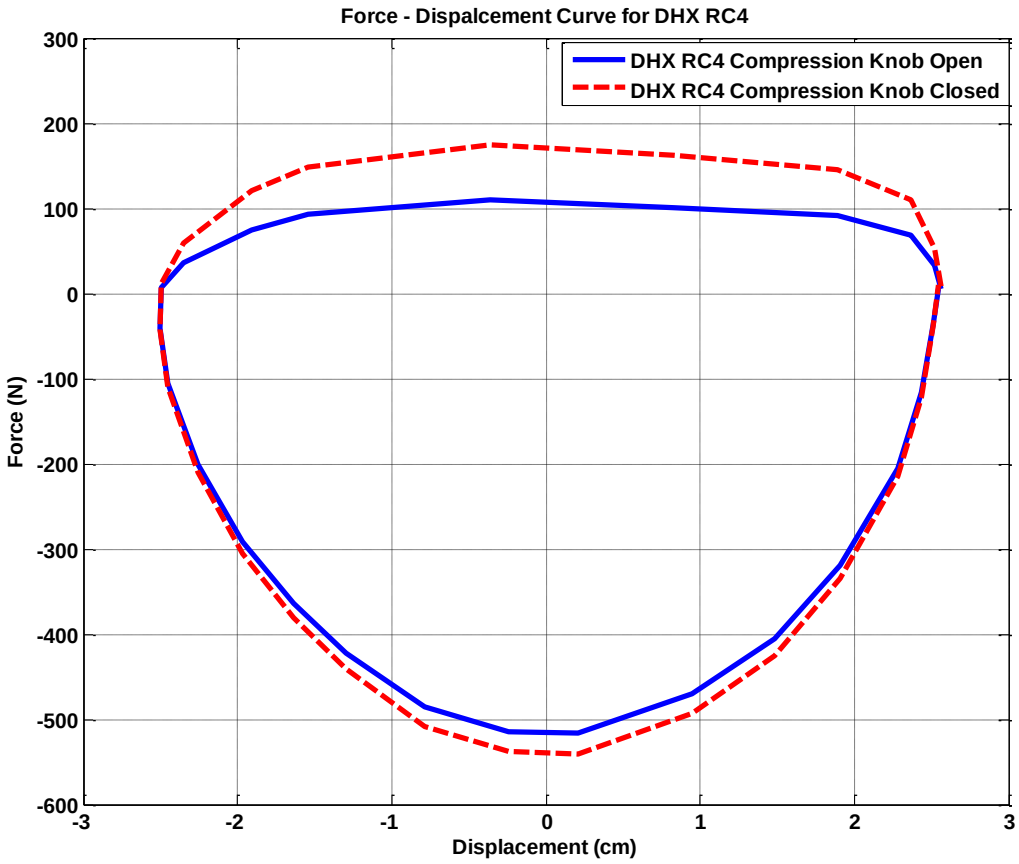

Figure 5.2 Force-displacement curves for a commercial DHX RC4 damper.

The approach here is to prove that MR technology is able to provide the same range of force on compression side without affecting the adjustability of the force on the rebound side. For this purpose the Zebra valve configuration will be used. The Zebra valve is a novel configuration for MR valves that improves the dynamic range of MR damper significantly. Based on our tests this damper improves the dynamic range of MR dampers up to 100% in fixed size, weight and dimensions. Moreover, Zebra configuration is compatible with AlNiCo magnets as explained in [77]. This leads to significantly lower energy consumption and higher lifetime of the batteries. AlNiCo powered MR dampers will

not require continuous electric current as they employ the magnetic characteristics of the AlNiCo to generate magnetic field without supplying electricity. This feature will address two of the major challenges of using MR technology in portable systems, first is the energy consumption and second one is the excess heat generation that defects the MR effect in MR dampers.

The Zebra valve should be retrofitted into the damper. The proposed design comprises a Zebra valve installed underneath the gas chamber of the DHX RC4 as shown in Fig 5.3.

Figure 5.3 The proposed concept for MR-based mountain bike damper.

The modeling of this sort of damping mechanism is slightly different with the common method explained in chapter 2. The quasi-static model explained in chapter 2 assumes the MR valve is a moving part installed as a piston while in the proposed configuration in this chapter the Zebra MR valve is stationary and the fluid passes through that. The equivalent velocity of the fluid passed through the Zebra valve can be calculated using the formula (5.1) and (5.2). This can be derived considering the volume change in the fluid chamber due to the movement of the damper rod in quasi-static movement.

$$\pi R_s^2 \dot{X}_p = \pi R_{ig}^2 \dot{X}_g \qquad (5.1)$$

Hence

$$\dot{X}_g = -\frac{\pi R_s^2 V_1}{\pi R_{ig}^2} = -\frac{R_s^2}{R_{ig}^2}\dot{X}_p \qquad (5.2)$$

In formulas (5.1) and (5.2) $\boldsymbol{R_s}$ represents the radius of the damper rod (shaft) , $\dot{X}_g$ is the equivalent velocity on the gas chamber side and the R_{ig} is the inner radius of the secondary chamber. Using the formula (5.2) the quasi static model can be rewritten as :

$$F_g = A_s P_a = A_s P_0 \left(\frac{V_0}{V_0 + A_s x_p}\right)^{\gamma} \qquad (5.3)$$

$$F_{vis} = \frac{12\,\eta L}{\pi {t_g}^3 R_d}\left(A_{zp}\right)^2\left(\dot{X}_g\right) \qquad (5.4)$$

$$F_{MR} = 2c\frac{L_p}{t_g}\,\tau_y\,(A_{zv})sgn\left(\dot{X}_g\right) \qquad (5.5)$$

In this formula A_{zp} represents the cross-section area of the Zebra valve.

By substituting (5.2) into (5.4) and (5.5):

$$F_{vis} = \frac{12\,\eta L}{\pi {t_g}^3 R_d}\left(A_{zp}\right)^2\left(-\frac{R_s^2}{R_{ig}^2}\,\dot{X}_p\right) \qquad (5.6)$$

$$F_{MR} = -2c\frac{L_p}{t_g}\,\tau_y\,(A_{zp})sgn\left(-\frac{R_s^2}{R_{ig}^2}\,\dot{X}_p\right) \qquad (5.7)$$

Using these formulas the off-state force and the MR effect force for Zebra valve can be calculated in stationary mode. . Using (5.6) and (5.7) the calculated off-state force

and MR effect force for an optimally designed Zebra valve filled with MRF 140CG at the velocity of 0.25 m/s are obtained as 68 N and 104 N, respectively. The calculated MR effect force is larger than the dynamic range of a DHX RC4 damper which was measured to be 72 N. The calculated MR effect force is larger than the dynamic range of a DHX RC4 damper. Thus, it is expected that employing Zebra valve can address the design objective which was matching the DHX RC4 dynamic range on compression side using the MR technology. In addition to the MR effect force the Zebra valve also adds an offset into the off-state force due to hydraulic effects; this extra force can be compensated by adjusting the shim stacks on the piston.

The Zebra valve should be redesigned in a way that it can be retrofitted on the DHX RC4 gas chamber. For this purpose the Zebra valve was redesigned by adding an additional cylindrical sleeve that could hold the Zebra valve in place. The drawing of this design can be seen in Fig 5.4.

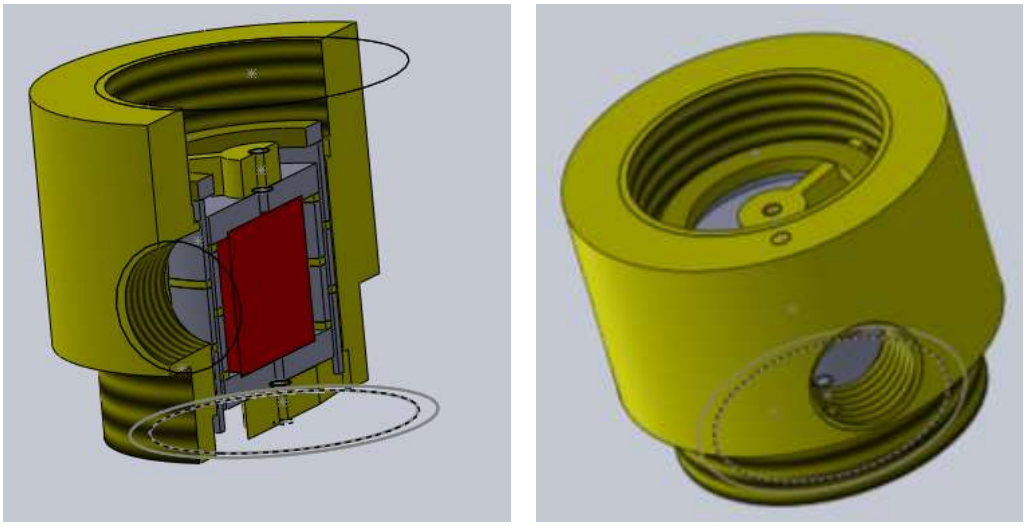

Figure 5.4 Drawing of the redesigned Zebra valve concept for mountain bikes.

In Fig 5.4 the yellow color represents Aluminum; red is AlNiCo and grey is Iron 1018. These parts are held together using a centric screw. The screw should be made of non-magnetic materials such as brass, aluminum or stainless steel 316 in order to avoid magnetic field bypassing the valve. In this case we used a 4-48 screw made of stainless steel 316 to have the non-magnetic features and tensile strength at the same time. The designed Zebra valve was built and assembled. The parts after manufacturing can be seen in Fig. 5.5.

Figure 5.5 Zebra valve parts after manufacturing.

The coil was wounded with 225 turns of AWG 28 enameled wires and the parts were assembled to each other. The assembled valve was fixed in the sleeve using epoxy and the entire part was installed on the damper. The DHX RC4 damper was filled with MRF 140CG. The assembled damper can be seen Fig. 5.6.

Figure 5.6 Assembled Zebra valve damper filled with MRF 140CG.

5.4. Characterization of the Damper:

In order to verify the design objective achievement characterization of the designed damper was necessary. The damper was tested in a standard condition using a Roehrig shaker. The gas chamber pressure was set to 827 kPa (120 psi), the temperature of the damper was set to 32.2C (90 F) degrees centigrade and the damper was shaken with sinusoidal movement with amplitude of 2.54cm (1 inch) and frequency of 10 Hz. The results obtained on the compression side for on-state and off-state can be seen in Fig 5.7. It is worth mentioning that the number of shims was adjusted before the test to make sure the off-state force of the damper equipped with Zebra Valve matches the off-state force of the conventional DHX RC4.

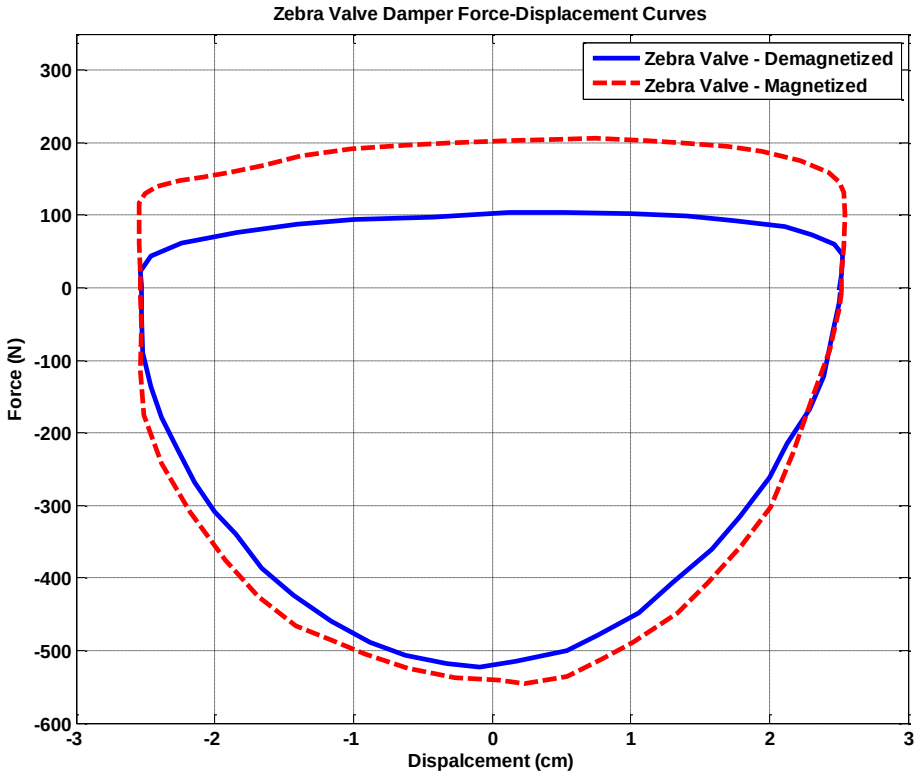

Figure 5.7 Force - Displacement curve for the Zebra valve damper in off (blue) and on state (red).

As it can be seen in Fig 5.7 the dynamic range of the Zebra equipped damper is about 40 Lbs which is about 60 percent more than the conventional DHX RC4 damper. On the rebound side the force could be adjusted anywhere between 100lbs to 450 Lbs using the built-in knob. As mentioned earlier the aim here is to control the compression force since that is the force that more often needs to be tuned. The rebound force though is tuned less often that can be done offline before the ride based on the rider's preferences. For the sake of switching the magnetic circuit on and off an electronic interface was employed that will further be explained in the next section.

The characterization was also done using a real world test bed to compare the performance of designed Zebra valve damper with the conventional DHX RC4 damper. The test bed can be seen in Fig. 5.8. This setup is equipped with two displacement

sensors and two accelerometers to measure the base excitation and the transmitted displacement and acceleration to the rider.

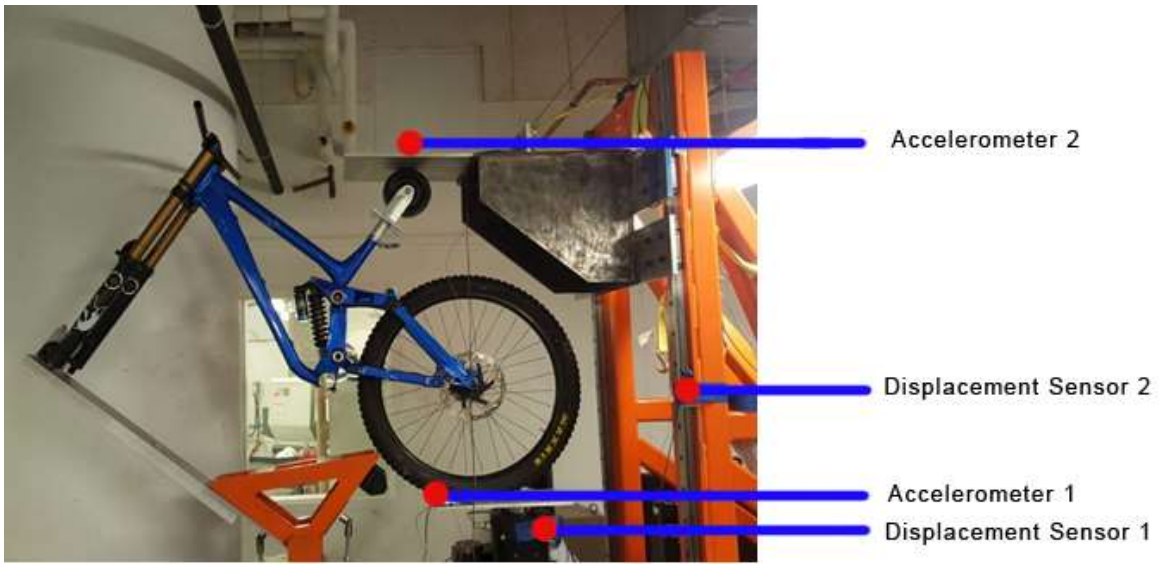

Figure 5.8 The vibration test-bed with a Maiden downhill bike installed on it.

In this setup the weight on the saddle of the bike was set to 75kg that represents the weight of a typical rider. The weight slides up and down as the base is excited and the displacement and acceleration are recorded. The results for the conventional DHX RC4 damper and the Zebra damper while the compression and rebound valves are both open can be seen in Fig. 5.9 and Fig. 5.10.

Both dampers were set to be fully open on compression and rebound side so the damping would be maximum and the bike will go back to its equilibrium point as fast as possible since the rebound force is also set to minimum. The test was done with a sinusoidal base excitation with an amplitude of 0.02 m at three different frequencies, 1, 2 and 3 Hz. It can clearly be seen that the two dampers have a very similar characteristics both in the transmitted displacement and transferred acceleration.

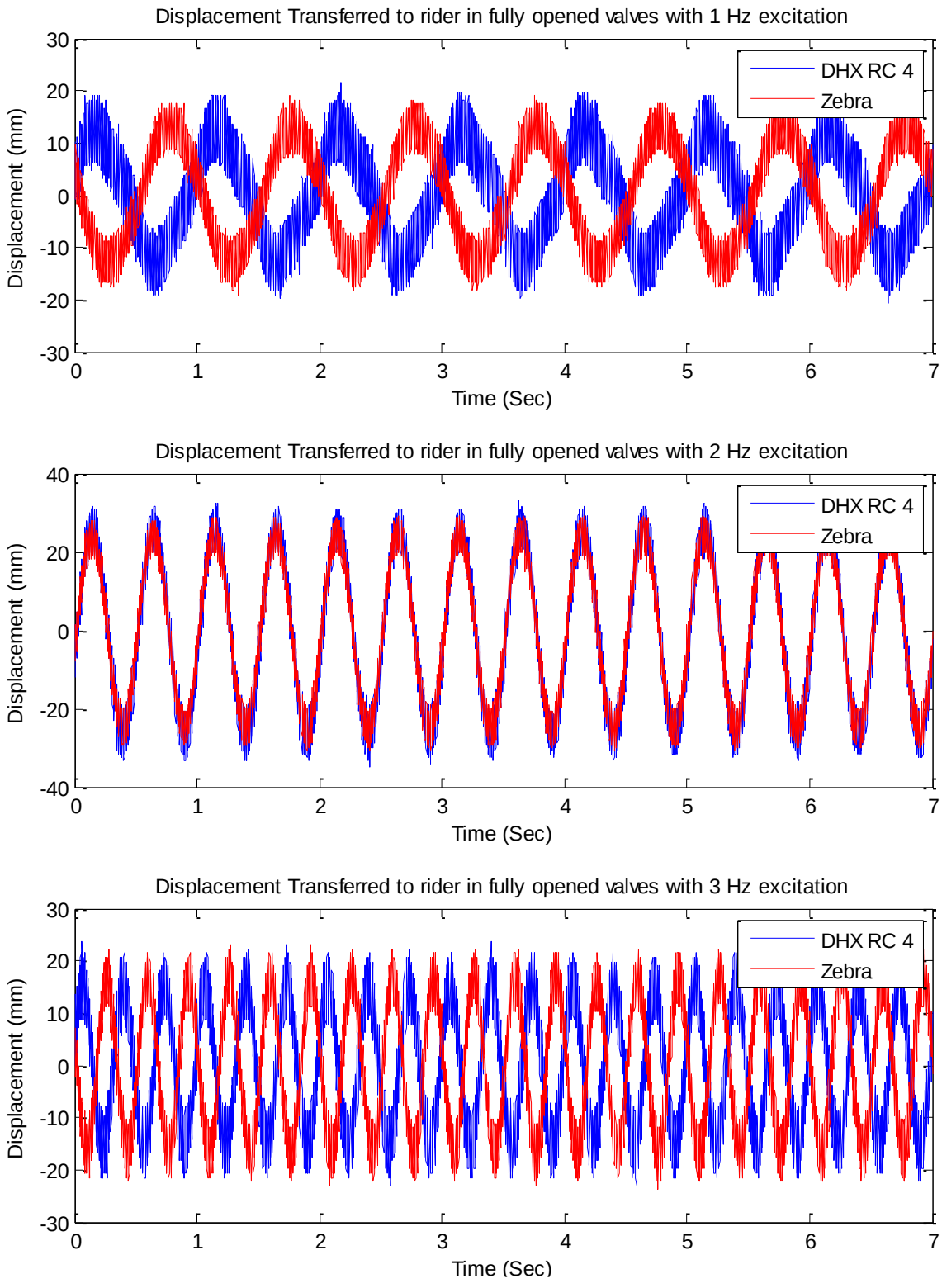

Figure 5.9 Displacement transmissibility for DHX RC4 and Zebra dampers in off-state (valves open).

.

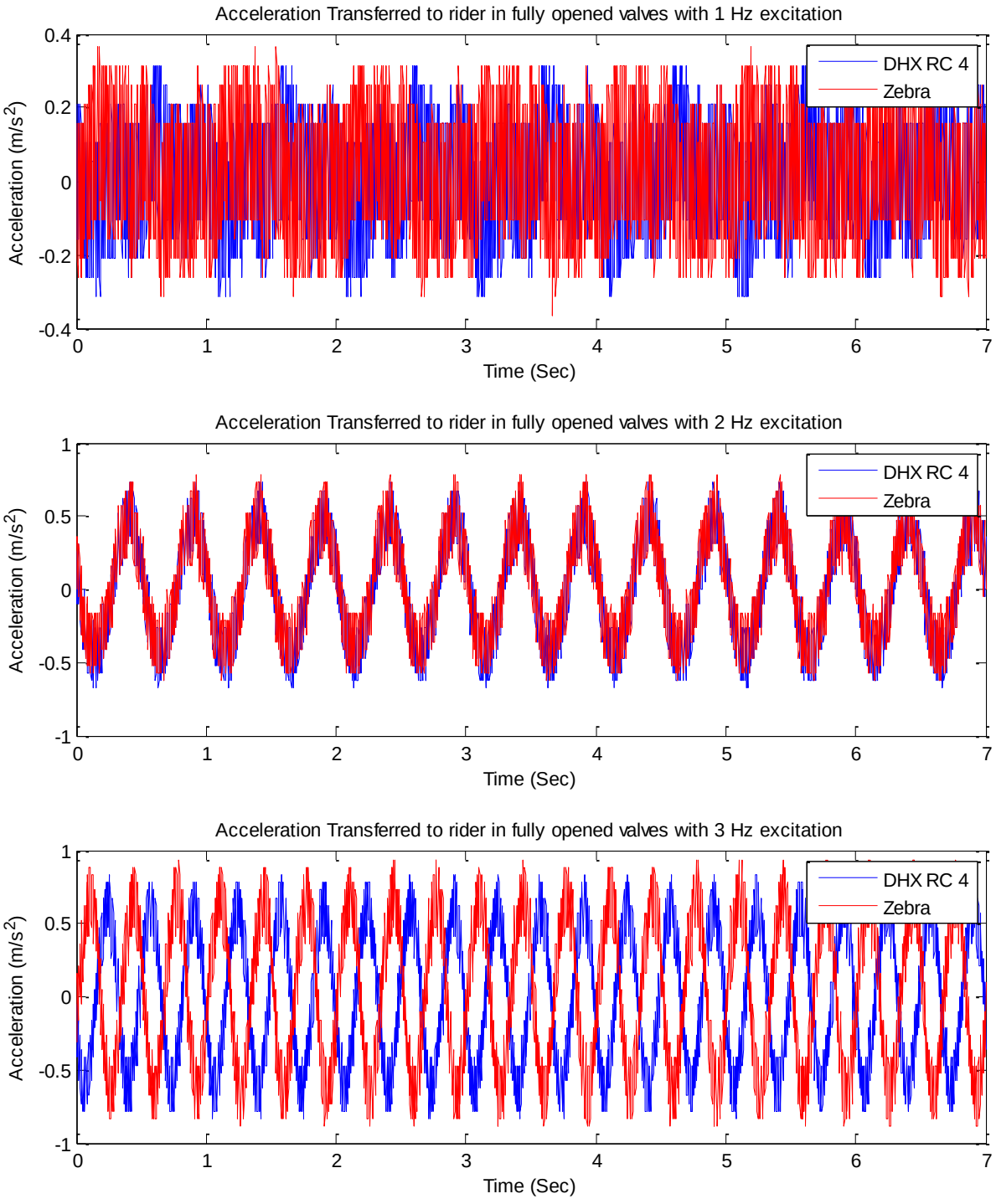

Figure 5.10 Acceleration transmissibility for DHX RC4 and Zebra dampers in off-state (valves open).

As it was seen in Fig. 5.9 and Fig. 5.10 and will be seen in the Fig. 5.11 and Fig. 5.12 a phase shift takes place as the excitation frequency changes. This effect is commonly seen in second order systems as the frequency gets closer to the resonance frequency. The present system, which consists of mass, spring and a damper, can be classified as a second order system.

So far it has been shown that the designed Zebra valve damper can match the required behaviour and characteristics in the off-state. To compare the performance of the Zebra Valve and DHX RC4 in the on state, the compression force for both dampers was set maximum. It was done by closing the compression knob for the DHX RC4 and activating the AlNiCo for the Zebra Valve. The results can be seen in Fig. 5.11 and Fig. 5.12. The test for the closed compression valve shows that the Zebra is able to perfectly match the characteristics of DHX RC4 and even in higher frequencies the transferred displacement and acceleration exceeds the measurements of the DHX RC4. This means Zebra can provider wider dynamic range comparing to DHX RC4. The two tests prove that the designed Zebra valve damper can match the off-state characteristics of the commercial DHX RC4 damper while it can beat that in dynamic range.

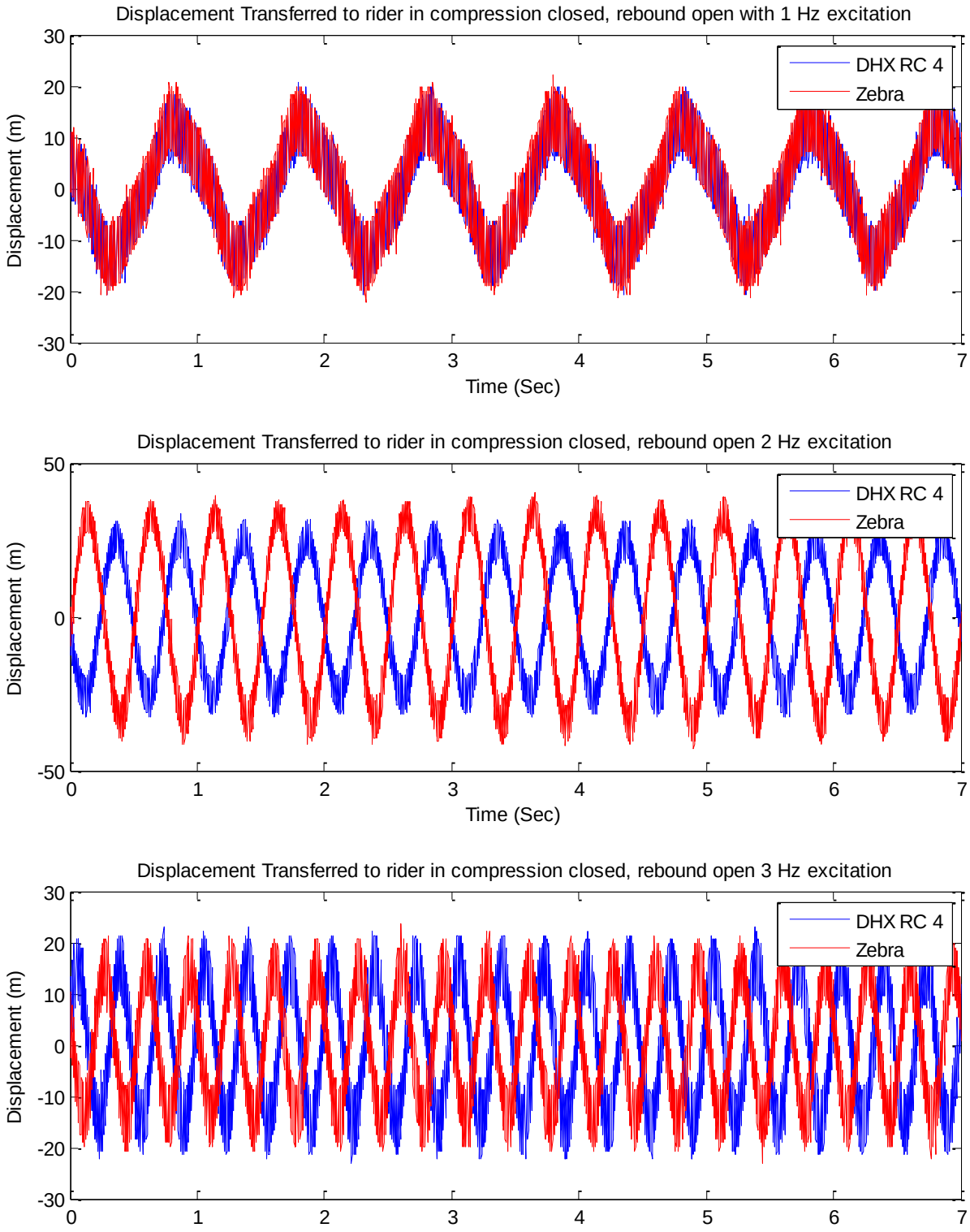

Figure 5.11 Displacement transmissibility for DHX RC4 and Zebra dampers in on-state (compression valve closed).

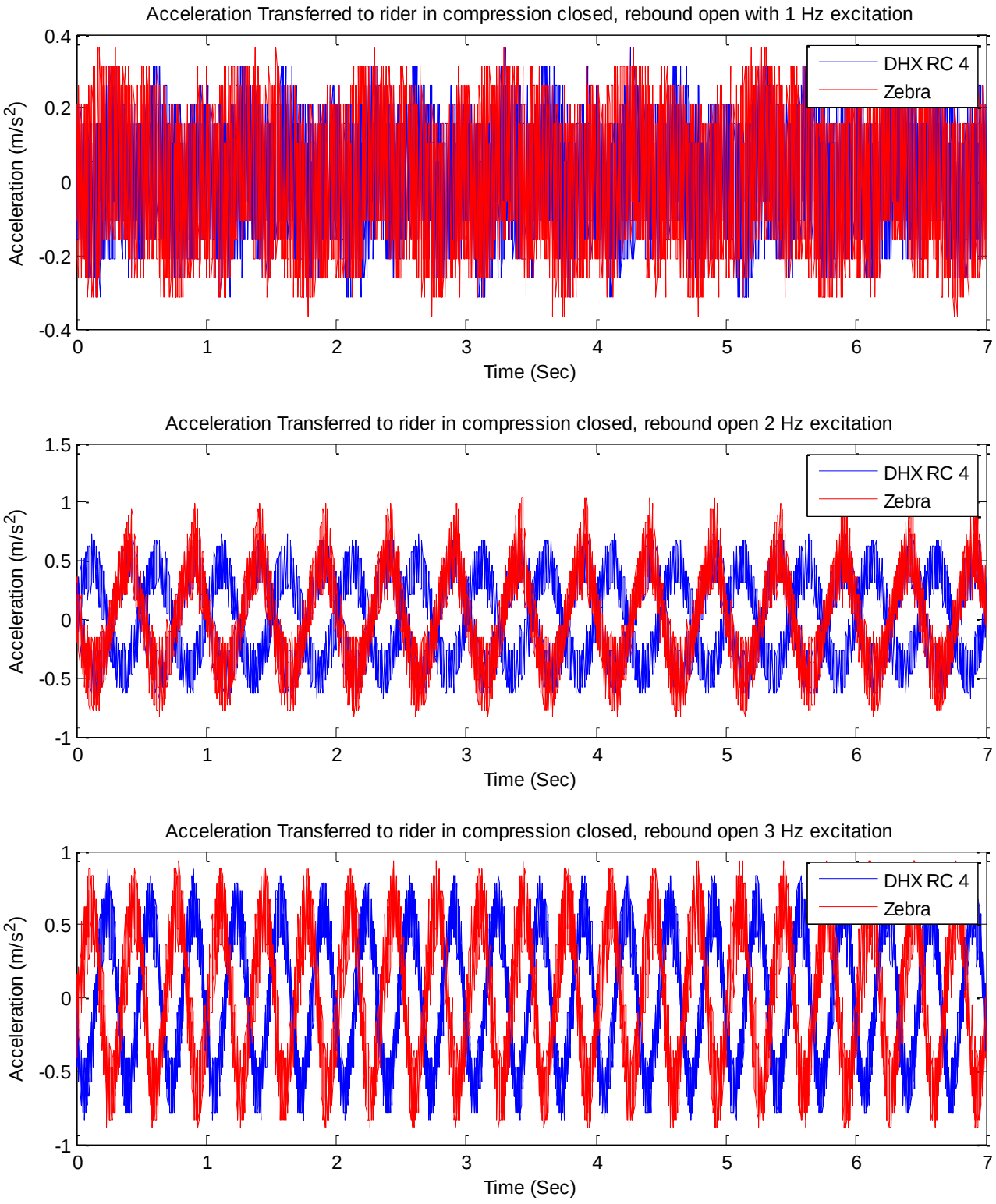

Figure 5.12 Acceleration transmissibility for DHX RC4 and Zebra dampers in on-state (compression valve closed).

5.5. Electronics

The MR dampers will require an Electronic Control Unit (ECU) to supply the power into the magnetic circuit. As discussed in section 4.6 the MR dampers with built-in AlNiCo will require more sophisticated control strategy. For this purpose an ECU was designed comprising of a battery stack, voltage regulator, power electronic h-brige and a microcontroller. The schematic of the designed ECU can be seen in Fig 5.13.

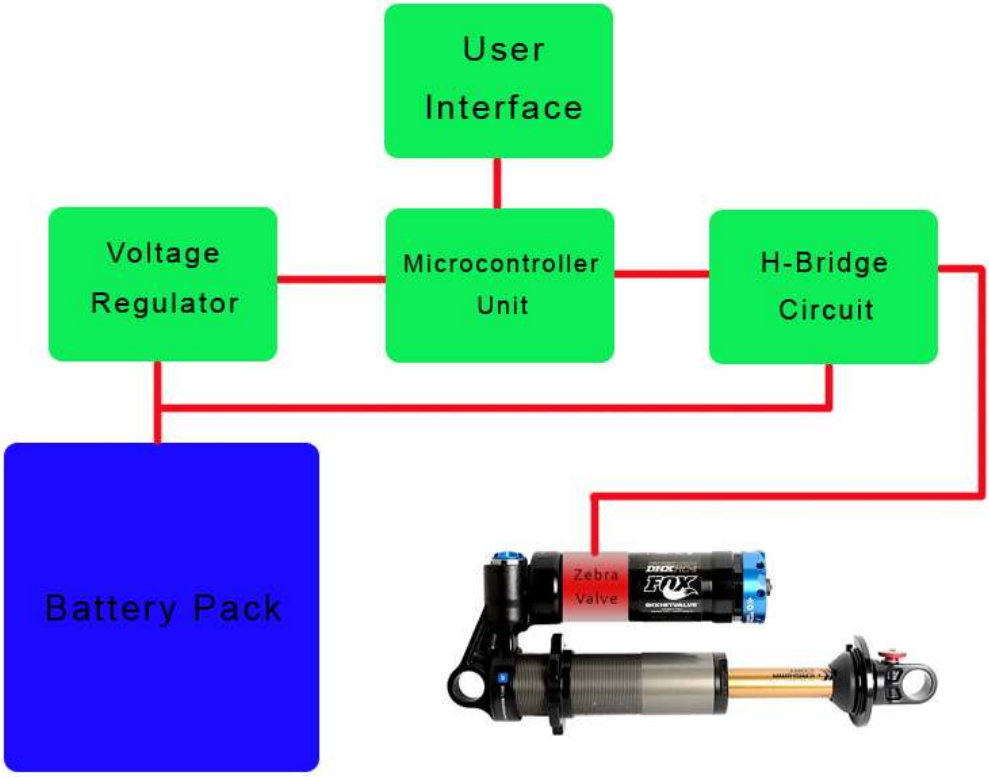

Figure 5.13 Schematic of the electronic control unit for the Zebra valve damper.

Based on the calculations, the required electric current for the electromagnet to operate is about 6.0 A. Considering the fact that the resistance of the coil is about 3 Ω the minimum required voltage is 18V. For this purpose six lithium ion batteries were stack

together to provide a nominal voltage of 22.2V. In order to supply the digital circuit, a voltage regulator is essential to produce 5V supply. For the sake of simplicity in this case an Arduino nano was used to implement the control scheme.

The AlNiCo magnet for magnetization and demagnetization requires bi-directional electric current which is achievable using h-bridge circuits. Considering the current and voltage ratings and the limited weight and space Pololu G2 2992 was chosen. This bridge converter is able to operate with currents and voltages up to 13A and 30V, respectively without requiring a heat sink.

The algorithm explained in section 4.6 was implemented on the microcontroller and the designed electronic circuit was installed on a Maiden mountain bike built by Rocky Mountain bikes as demonstrated in Fig 5.15.

Figure 5.14 The Zebra valve damper installed on a commercial Maiden bike with battery, electronics and user interface included.

5.6. Field Tests

To verify the functionality of the designed Zebra damper field tests were planned to be done by two professional riders in standard downhill biking trails in North Vancouver, Canada. In this test the bike shown in Fig 5.15 was rode for several times by different riders to see if any difference in performance is reported in comparison to a commercial damper. According to the riders, the designed Zebra valve damper does not have a noticeable difference with a conventional downhill bike damper in terms of forces felt on the pedals, handle bar and saddle while it has an added functionality that lets the rider adjust the compression force using a knob on the handle bar. The Fig. 5.16 demonstrates the bike with a Zebra valve damper installed on a downhill biking trail in North Vancouver, Canada.

Also, a financial analysis was also conducted to study the financial feasibility of the designed MR damper. A conventional mountain bike damper is sold at consumer price of several hundred dollars while the cost of manufacturing, labour and MR fluid for one single prototype was less than 200 Canadian dollars. For an industrial mass manufacturing, the cost can be decreased significantly. It can be concluded that the proposed technology can be applied to mountain bike dampers for commercial use.

Figure 5.15 The Maiden mountain bike with a Zebra valve damper installed on it in a downhill biking trail.

5.7. Conclusion

Asymmetric damping behavior is a necessary feature for commercial shock absorbers. This feature has not been very well foreseen in the design and development of MR dampers. In addition to asymmetric damping, MR dampers are inefficient in terms of mass, energy consumption, required space and the excess heat generation. In this research the shortcomings of MR dampers have been taken into account it has been tried to address all the challenges against applying MR technology in consumer products.

This study includes all the possibilities for hydraulic damping generation and has proposed a novel configuration, which is a combination of conventional hydraulic valves and novel MR technologies to address all the requirements for a commercial shock absorber. The proposed damper configuration employs the Zebra concept as a mass and energy efficient system for MR valves. Also, AlNiCo magnets have been employed in this design as an effective solution for minimizing the energy consumption and excess heat generation. The proposed design was utilized to design and fabricate an MR damper for mountain bike application. The designed damper was characterized and tested in lab condition and real world situation and the results were compared with a commercial damper of the same dimensions. It was shown that the proposed configuration is able to perfectly match the characteristics of the commercial damper and it can beat that in terms of the dynamic range and adjustability.

Chapter 6. Summary, Conclusion, and Suggestions for Future Works

6.1. Summary and Conclusion

In this thesis, the idea of developing a low-power light-weight MagnetoRheological damper was investigated. This was done by investigating various modeling methods and optimal design approaches and studying alternative configurations for high performance MR dampers for mass and energy sensitive applications. In addition, the utilization of MR dampers where asymmetric damping behavior is necessary was studied. The key contributions of the present dissertation can be summarized as follows:

1. A novel comprehensive optimal design approach was proposed for optimization of MR dampers. The proposed approach is an analytic solution to design MR dampers with multi-material structures that guarantees the global optimality of the solution while being computationally efficient. This approach was verified by design and fabrication of an MR damper with AlNiCo core.

2. An innovative configuration for MR dampers was proposed in this thesis. The proposed configuration addresses the mass and energy inefficiency of conventional MR dampers by significantly increasing the active magnetic area of contact and employing AlNiCo as a magnetic core. The proposed configuration was utilized to design and fabricate an MR damper that was compared with an optimally designed conventional MR damper with similar dimensions, weight and off-state force. It was shown that the proposed configuration is able to significantly increase the dynamic range. In this case

the designed MR damper could increase the dynamic range of the damper 100 percent while providing the same size, weight and characteristics.

3. In most applications it is essential that the dampers provide asymmetric damping characteristics. In this research an innovative solution was suggested to employ MR technology in applications with asymmetric damping requirements. The proposed solution was utilized to design and fabricate a downhill mountain bike suspension damper that could provide a wider dynamic range and relatively better performance while compared to a commercial downhill hydraulic damper.

The outcome of this dissertation provide a framework for design and fabrication of MR dampers for mass and energy sensitive applications such as robotics, mountain bikes, and prosthetics.

6.2. Suggestions for Future Works

Based on the experience gained and lessons learned over the course of this research the following activities may be considered for future works.

6.2.1. Design and Fabricate a Mass and Energy Efficient MR Damper for Automotive Applications

In this research a novel configuration for MR dampers was proposed that could significantly improve the performance and increase the energy efficiency of MR dampers. The proposed configuration was optimally designed using a novel optimal design approach for mountain bike applications. The same process can be followed to design an efficient high performance MR damper for automotive applications. Specially in the field

of Electric Vehicles (EV) where weight and energy consumptions are of concern this configuration can be very useful.

The other factor that makes this novel configuration more attractive in the field of EVs is the fact that these vehicles are design to be light. Lower weight results in less effective performance of conventional hydraulic suspension systems. The proposed MR damper concept as a high performance low-power, light-weight semi-active suspension solution can significantly improve the performance in EVs.

6.2.2. Improve Energy Efficiency

In this research the focus was design and implement a novel concept for MR dampers and energy efficiency of the power electronics and battery system was not investigated in detail. It is suggested that the control system to be optimized in following terms:

1. Employ model-based control solutions to control the magnetization of AlNiCo without exciting that into saturation. This can significantly improve the energy efficiency.

2. Regenerating the excitation current supplied into the electromagnetic coil.

3. Employ boost converters to further decrease the required battery voltage and decrease the overall weight of the system.

6.2.3. Adaptive Damping Control System Design

It is suggested that an adaptive damping control system be developed which is able to fulfill following functionalities:

1. Sense the pedaling behavior of the rider and adjust the damping so that the rider's effort dissipation while pedaling in minimized in the damper and overall performance is improved.

2. Sense the terrain, road roughness and base induced vibration using an ultrasound sensor or through a sensor installed on the front fork and adjust the damping of the rear shock absorber to increase the handling and ride comfort for the rider.

3. Sense the temperature of the damper and adjust the damping to assure consistent damping characteristics to match the preferences of the rider. A common effect seen in mountain bike dampers, called fade out effect, happens when the temperature of the damper increases which leads to a decrease of hydraulic fluid viscosity. This undesirable effect can be compensated by utilizing the MR effect force through magnetizing the electromagnetic coil to a certain point based on the damper temperature.

References

[1] J. D. Carlson and M. R. Jolly, “MR fluid, foam and elastomer devices,” *Mechatronics*, vol. 10, no. 4, pp. 555–569, 2000.

[2] K. Oliveira, M. César, and J. Gonçalves, “Fuzzy Based Control of a Vehicle Suspension System Using a MR Damper,” *Control. 2016*, 2017.

[3] L. Balamurugan, J. Jancirani, and M. A. Eltantawie, “Generalized magnetorheological (MR) damper model and its application in semi-active control of vehicle suspension system,” *Int. J. Automot. Technol.*, vol. 15, no. 3, pp. 419–427, 2014.

[4] J. Chen, X. Z. Jiang, and N. Xu, “Semi-Active Control of a Vehicle Suspension Based on Magneto-Rheological Damper,” *Adv. Mater. Res.*, vol. 311–313, pp. 2286–2290, 2011.

[5] A. Yilmaz, A. Sadeghimorad, I. Şahin, and Z. Evren Kaya, “Analysis of the performance of controlled semi-active knee joint with magnetorheological (MR) damper,” in *2014 18th National Biomedical Engineering Meeting, BIYOMUT 2014*, 2003.

[6] J. Park, J. Kang, and S. Choi, “Design and Analysis of Above Knee Prosthetic Leg Using MR Damper,” *Trans. Korean Soc. Noise Vib. Eng.*, vol. 26, no. 2, pp. 165–171, 2016.

[7] F. Gao, Y. N. Liu, and W. H. Liao, “Optimal design of a magnetorheological damper used in smart prosthetic knees,” *Smart Mater. Struct.*, vol. 26, no. 3,

2017.

[8] B. F. S. J. S J Dyke M K Sain and J D Carlson, “Modeling and control of magnetorheological dampers for seismic response reduction-1996.pdf,” *Smart Mater. Struct.*, no. 5, pp. 565–575, 1996.

[9] A. Friedman *et al.*, “Large-Scale Real-Time Hybrid Simulation for Evaluation of Advanced Damping System Performance,” *J. Struct. Eng.*, vol. 141, no. 6, p. 4014150, 2015.

[10] Y.-T. Choi and N. M. Wereley, “Vibration Control of a Landing Gear System Featuring Electrorheological/Magnetorheological Fluids,” *J. Aircr.*, vol. 40, no. 3, pp. 432–439, 2003.

[11] W. Hu and N. Wereley, “Magnetorheological fluid and elastomeric lag damper for helicopter stability augmentation,” *Int. J. Mod. Phys. B*, 2005.

[12] J. D. Carlson, D. M. Catanzarite, and K. A. St. Clair, “COMMERCIAL MAGNETO-RHEOLOGICAL FLUID DEVICES,” *Int. J. Mod. Phys. B*, vol. 10, no. 23n24, pp. 2857–2865, Oct. 1996.

[13] M. R. Jolly, J. W. Bender, and J. D. Carlson, “Properties and applications of commercial magnetorheological fluids,” 1998, vol. 3327, pp. 262–275.

[14] Q.-H. Nguyen and S.-B. Choi, “Optimal Design Methodology of Magnetorheological Fluid Based Mechanisms,” *Smart Actuation Sens. Syst. – Recent Adv. Futur. Challenges Des.*, pp. 347–382, Oct. 2012.

[15] Q. H. Nguyen, S. B. Choi, and K. S. Kim, “Geometric optimal design of MR damper considering damping force, control energy and time constant,” *J. Phys.*

Conf. Ser., vol. 149, p. 12076, Feb. 2009.

[16] H. Gavin, J. Hoagg, and M. Dobossy, “Optimal design of MR dampers,” *Proc. US-Japan Work. Smart Struct. Improv. Seism. Perform. Urban Reg.*, no. August, pp. 225–236, 2001.

[17] X. Song, M. Ahmadian, and S. C. Southward, “Modeling magnetorheological dampers with application of nonparametric approach,” *J. Intell. Mater. Syst. Struct.*, vol. 16, no. 5, pp. 421–432, May 2005.

[18] X. C. Guan and P. F. Guo, “Modeling of magnetorheological dampers utilizing a general non-linear model,” in *Journal of Intelligent Material Systems and Structures*, 2011, vol. 22, no. 5, pp. 435–442.

[19] J.-H. Yoo and N. M. Wereley, “Design of a High-Efficiency Magnetorheological Valve,” *J. Intell. Mater. Syst. Struct.*, vol. 13, no. 10, pp. 679–685, Oct. 2002.

[20] M. E. Uz and M. N. S. Hadi, “Optimal design of semi active control for adjacent buildings connected by MR damper based on integrated fuzzy logic and multi-objective genetic algorithm,” *Eng. Struct.*, vol. 69, pp. 135–148, 2014.

[21] A. Mahmoudi, S. Kahourzade, N. A. Rahim, and W. P. Hew, “Design, Analysis, and Prototyping of an Axial-Flux Permanent Magnet Motor Based on Genetic Algorithm and Finite-Element Analysis,” *IEEE Trans. Magn.*, vol. 49, no. 4, pp. 1479–1492, Apr. 2013.

[22] N. M. Kwok, Q. P. Ha, M. T. Nguyen, J. Li, and B. Samali, “Bouc–Wen model parameter identification for a MR fluid damper using computationally efficient GA,” *ISA Trans.*, vol. 46, no. 2, pp. 167–179, Apr. 2007.

[23] N. Institution of Electrical Engineers. and S. Bolognani, *IEE proceedings. Electric power applications.*, vol. 145, no. 5. Institution of Electrical Engineers, 1994.

[24] B. Assadsangabi, F. Daneshmand, N. Vahdati, M. Eghtesad, and Y. Bazargan-Lari, “Optimization and design of disk-type MR brakes,” *Int. J. Automot. Technol.*, vol. 12, no. 6, pp. 921–932, Dec. 2011.

[25] Q. H. Nguyen and S. B. Choi, “Optimal design of a vehicle magnetorheological damper considering the damping force and dynamic range,” *Smart Mater. Struct.*, vol. 18, no. 1, p. 15013, Jan. 2009.

[26] Q. H. Nguyen and S. B. Choi, “Optimal design of an automotive magnetorheological brake considering geometric dimensions and zero-field friction heat,” *Smart Mater. Struct.*, vol. 19, no. 11, p. 115024, Nov. 2010.

[27] L. Davis, *Handbook of genetic algorithms*. Van Nostrand Reinhold, 1991.

[28] C. Load, “MRF-132DG Magneto-Rheological Fluid,” *Lord product selector guide: lord magnetorheological fluids*, vol. 54, no. 2. p. 11, 2011.

[29] Kerem Karakoc, “Design of a Magnetorheological Brake System Based on Magnetic Circuit Optimization,” University of Victoria, 2007.

[30] Katsuhiko Ogata, *Modern Control Engineering*, 5th ed. Pearson, 2010.

[31] Y. Xu, M. Ahmadian, and R. Sun, “Improving vehicle lateral stability based on variable stiffness and damping suspension system via MR damper,” *IEEE Trans. Veh. Technol.*, vol. 63, no. 3, pp. 1071–1078, Mar. 2014.

[32] K. Kim and D. Jeon, “Vibration suppression in an MR fluid damper suspension

system," *J. Intell. Mater. Syst. Struct.*, vol. 10, no. 10, pp. 779–786, Oct. 1999.

[33] Y. Ding, L. Zhang, H. T. Zhu, and Z. X. Li, "A new magnetorheological damper for seismic control," *Smart Mater. Struct.*, vol. 22, no. 11, p. 115003, Nov. 2013.

[34] B. Chen, Y.-Z. Sun, Y.-L. Li, and S.-L. Zhao, "Control of Seismic Response of a Building Frame by Using Hybrid System with Magnetorheological Dampers and Isolators," *Adv. Struct. Eng.*, vol. 17, no. 8, pp. 1199–1215, Aug. 2014.

[35] J. Z. Chen and W. H. Liao, "Design , testing and control of a magnetorheological actuator for assistive," *Smart Mater. Struct.*, vol. 35029, no. 3, p. 35029, Mar. 2010.

[36] T. C. Bulea, R. Kobetic, C. S. To, M. L. Audu, J. R. Schnellenberger, and R. J. Triolo, "A variable impedance knee mechanism for controlled stance flexion during pathological gait," *IEEE/ASME Trans. Mechatronics*, vol. 17, no. 5, pp. 822–832, Oct. 2012.

[37] Q. H. Nguyen, S. B. Choi, and J. K. Woo, "Optimal design of magnetorheological fluid-based dampers for front-loaded washing machines," *Proc. Inst. Mech. Eng. Part C J. Mech. Eng. Sci.*, vol. 228, no. 2, pp. 294–306, Feb. 2014.

[38] E. J. Park, L. F. da Luz, and A. Suleman, "Multidisciplinary design optimization of an automotive magnetorheological brake design," *Comput. Struct.*, vol. 86, no. 3–5, pp. 207–216, Feb. 2008.

[39] A. Hadadian, R. Sedaghati, and E. Esmailzadeh, "Design optimization of magnetorheological fluid valves using response surface method," *J. Intell. Mater. Syst. Struct.*, vol. 25, no. 11, pp. 1352–1371, Jul. 2014.

[40] Z. Parlak, T. Engin, and İ. Çallı, “Optimal design of MR damper via finite element analyses of fluid dynamic and magnetic field,” *Mechatronics*, vol. 22, no. 6, pp. 890–903, Sep. 2012.

[41] X. Zhu, X. Jing, and L. Cheng, “Optimal design of control valves in magnetorheological fluid dampers using a nondimensional analytical method,” *J. Intell. Mater. Syst. Struct.*, vol. 24, no. 1, pp. 108–129, Jan. 2013.

[42] Q. H. Nguyen, S. B. Choi, Y. S. Lee, and M. S. Han, “An analytical method for optimal design of MR valve structures,” *Smart Mater. Struct.*, vol. 18, no. 9, p. 95032, Sep. 2009.

[43] H. Böse and J. Ehrlich, “Magnetorheological dampers with various designs of hybrid magnetic circuits,” in *Journal of Intelligent Material Systems and Structures*, 2012, vol. 23, no. 9, pp. 979–987.

[44] L. Huang, J. Li, and W. Zhu, “Mathematical model of a novel small magnetorheological damper by using outer magnetic field,” *AIP Adv.*, vol. 7, no. 3, p. 35114, Mar. 2017.

[45] D. Case, B. Taheri, and E. Richer, “Dynamical Modeling and Experimental Study of a Small-Scale Magnetorheological Damper,” *IEEE/ASME Trans. Mechatronics*, vol. 19, no. 3, pp. 1015–1024, Jun. 2014.

[46] GORDANINEJAD FARAMARZ; BREESE DARRELL G, “Magneto-rheological fluid damper,” 2000.

[47] B. S. Janusz Goldasz, *INSIGHT INTO MAGNETORHEOLOGICAL SHOCK ABSORBERS Download : Insight Into Magnetorheological Shock Absorbers*.

2015.

[48] J. Goldasz, “Electro-mechanical analysis of a magnetorheological damper with electrical steel laminations,” *Przegląd Elektrotechniczny*, no. 2, pp. 8–12, 2013.

[49] S. Sassi, K. Cherif, L. Mezghani, M. Thomas, and A. Kotrane, “An innovative magnetorheological damper for automotive suspension: From design to experimental characterization,” *Smart Mater. Struct.*, vol. 14, no. 4, pp. 811–822, Aug. 2005.

[50] F. R. BUSCHOW, K.H.J.; DE BOER, *Physics of Magnetism and Magnetic Materials.* Kluwer Academic/Plenum Publishers, 2004.

[51] A. N. (Ara N. 1977- Knaian, “Electropermanent magnetic connectors and actuators : devices and their application in programmable matter,” 2010.

[52] L. Masisi, M. Ibrahim, and P. Pillay, “Control strategy of a variable flux machine using AlNiCo permanent magnets,” in *2015 IEEE Energy Conversion Congress and Exposition, ECCE 2015*, 2015, pp. 5249–5255.

[53] M. Ibrahim, L. Masisi, and P. Pillay, “Design of Variable-Flux Permanent-Magnet Machines Using Alnico Magnets,” *IEEE Trans. Ind. Appl.*, vol. 51, no. 6, pp. 4482–4491, Nov. 2015.

[54] Y. Sato and S. Umebara, “Power-saving magnetization for magnetorheological fluid control using a combination of permanent magnet and electromagnet,” *IEEE Trans. Magn.*, vol. 48, no. 11, pp. 3521–3524, Nov. 2012.

[55] “Grades of Alnico.” [Online]. Available: http://e-magnetsuk.com/alnico_magnets/alnico_grades.aspx. [Accessed: 12-Apr-2017].

[56] Y. Bernard, E. Mendes, and F. Bouillault, “Dynamic hysteresis modeling based on Preisach model,” in *IEEE Transactions on Magnetics*, 2002, vol. 38, no. 2 I, pp. 885–888.

[57] J. Tellinen, “Simple scalar model for magnetic hysteresis,” *IEEE Trans. Magn.*, vol. 34, no. 4 pt 2, pp. 2200–2206, Jul. 1998.

[58] E. Burke, *High-tech cycling*. Human Kinetics, 2003.

[59] K. P. Balike, S. Rakheja, and I. G. Stiharu, “Optimal synthesis of a two-stage asymmetric damper of an automotive suspension considering wheel camber variations,” *Proc. Inst. Mech. Eng. Part D J. Automob. Eng.*, vol. 225, no. 8, pp. 1006–1022, Aug. 2011.

[60] A. S. M. S. Islam and A. K. W. Ahmed, “A Comparative Study of Advanced Suspension Dampers for Vibration and Shock Isolation Performance of Road Vehicle,” *SAE 2006 Trans. J. Passeng. Cars Mech. Syst.*, Apr. 2006.

[61] N. Eslaminasab, S. Arzanpour, and M. F. Golnaraghi, “Optimal Design of Asymmetric Passive and Semi-Active Dampers,” in *Volume 9: Mechanical Systems and Control, Parts A, B, and C*, 2007, pp. 1841–1847.

[62] W. Wanjun, Z. Weigong, and W. Enrong, “Generation and Modeling of Asymmetric Hysteresis Damping Characteristics for a Symmetric Magnetorheological Damper,” in *2009 Second International Conference on Intelligent Computation Technology and Automation*, 2009, pp. 184–189.

[63] J. Y. (Jo Y. Wong, *Theory of ground vehicles*. Wiley, 2008.

[64] R. Redfield, “Large motion mountain biking dynamics,” *Veh. Syst. Dyn.*, vol. 43,

no. 12, pp. 845–865, Dec. 2005.

[65] O. Faiss, R; Praz, M; Meichtry, A; Gobelet, C; Deriaz, “The effect of mountain bike suspensions on vibrations and off-road uphill performance,” *J. Sports Med. Phys. Fitness*, vol. 47, no. 2, pp. 151–8, 2007.

[66] J. Seifert, M. Luetkerneier, M. Spencer, D. Miller, and E. Burke, “The Effects of Mountain Bike Suspension Systems on Energy Expenditure, Physical Exertion, and Time Trial Performance During Mountain Bicycling,” *Int. J. Sports Med.*, vol. 18, no. 3, pp. 197–200, Apr. 1997.

[67] H.-H. MacRae HS-H, K. J. Hise, and P. J. Allen, “Effects of front and dual suspension mountain bike systems on uphill cycling performance.,” *Med. Sci. Sports Exerc.*, vol. 32, no. 7, pp. 1276–80, Jul. 2000.

[68] K. Nishii, T; Umemura, Y; Kitagawa, “Full suspension mountain bike improves off-road cycling performance,” *J. Sports Med. Phys. Fitness*, vol. 44, no. 4, pp. 356–60, 2004.

[69] C.-C. Wu, “Static and dynamic analyses of mountain bikes and their riders,” University of Glasgow, 2013.

[70] M. González, J. Cuadrado, F. González, and D. Dopico, “Optimization of an off-road bicycle with four-bar linkage rear suspension,” vol. 8, pp. 2–8, 2008.

[71] D. G. Breese and F. Gordaninejad, “Semi-active, fail-safe magneto-rheological fluid dampers for mountain bicycles,” *Int. J. Veh. Des.*, vol. 33, no. 1–3, pp. 128–138, 2003.

[72] F. Gordaninejad and D. G. Breese, “Heating of Magnetorheological Fluid

Dampers," *J. Intell. Mater. Syst. Struct.*, vol. 10, no. 8, pp. 634–645, Aug. 1999.

[73] D. C. Batterbee and N. D. Sims, "Magnetorheological platform dampers for mountain bikes," in *Proceedings Volume 7290, Industrial and Commercial Applications of Smart Structures Technologies 2009*, 2009.

[74] S.-B. Choi, S.-R. Hong, C.-C. Cheong, and Y.-K. Park, "Comparison of Field-Controlled Characteristics between ER and MR Clutches," *J. Intell. Mater. Syst. Struct.*, vol. 10, no. 8, pp. 615–619, Aug. 1999.

[75] "Lapierre and RockShox launch auto-adjust suspension - BikeRadar." [Online]. Available: https://www.bikeradar.com/news/article/lapierre-and-rockshox-launch-auto-adjust-suspension-34390/. [Accessed: 25-May-2018].

[76] "SHOCK- 2014 FLOAT iCD | Bike Help Center | FOX." [Online]. Available: http://www.ridefox.com/fox17/help.php?id=69&m=bike. [Accessed: 25-May-2018].

[77] H. Böse and J. Ehrlich, "Magnetorheological dampers with various designs of hybrid magnetic circuits," in *Journal of Intelligent Material Systems and Structures*, 2012, vol. 23, no. 9, pp. 979–987.